Provenance history of detrital diamond deposits, West Coast of Namaqualand, South Africa

D. Phillips[1] • J.W. Harris[2] • M.C.J. de Wit[3] • E.L. Matchan[1]

✉ D. Phillips

dphillip@unimelb.edu.au

[1] School of Earth Sciences, The University of Melbourne, Parkville, VIC, 3010, Australia

[2] School of Geographical and Earth Sciences, University of Glasgow, Glasgow, G12 8QQ, United Kingdom

[3] Tsodilo Resources Limited., P.O. Box 508, Toronto, Ontario, M5J 2S1, Canada

Abstract The West Coast of Namaqualand in South Africa hosts extensive detrital diamond deposits, but considerable debate exists as to the provenance of these diamonds. Some researchers have suggested derivation of the diamonds from Cretaceous-Jurassic kimberlites (also termed Group I kimberlites) and orangeites (also termed Group II kimberlites) located on the Kaapvaal Craton. However, others favour erosion of diamonds from the ca.300 Ma Dwyka Group sediments, with older, pre-Karoo kimberlites being the original source(s). Previous work has demonstrated that $^{40}Ar/^{39}Ar$ analyses of clinopyroxene inclusions, extracted from diamonds, yield ages approaching the time(s) of source kimberlite emplacement, which can be used to constrain the provenance of placer diamond deposits. In the current study, $^{40}Ar/^{39}Ar$ analyses were conducted on clinopyroxene inclusions from two similar batches of

Namaqualand detrital diamonds, yielding (maximum) ages ranging from 117.5 ± 43.6 Ma to 3684 ± 191 Ma (2σ) and 120.6 ± 15.4 Ma to 688.8 ± 4.9 Ma (2σ), respectively. The vast majority of inclusions (88%) produced ages younger than 500 Ma, indicating that most Namaqualand diamonds originated from Cretaceous-Jurassic kimberlites/orangeites, with few, if any, derived from the Dwyka tillites. The provenance of the Namaqualand diamonds from ca.115-200 Ma orangeites is consistent with Late Cretaceous paleo-drainage reconstructions, as these localities could have been sampled by the 'paleo-Karoo' River and transported to the West Coast via an outlet close to the current Olifants River mouth. At ca.90 Ma, this drainage system appears to have been captured by the 'paleo-Kalahari' River, a precursor to the modern Orange River system. This latter drainage is considered to have transported diamonds eroded from both ca.80-90 Ma kimberlites and ca.115-200 Ma orangeites to the West Coast, which were subsequently reworked along the Namibian coast, forming additional placer deposits.

Key words:

diamond

kimberlite

$^{40}Ar/^{39}Ar$

provenance

Character count: 46,900 Characters (with spaces)

40,000 Characters (no spaces)

Introduction

The West Coast of southern Africa is host to the world's largest known detrital diamond deposits (Fig. 1). Together these deposits have produced in excess of 120 million carats of diamonds, with ~50 million carats from mines in Namaqualand, South Africa (e.g., Gurney et al., 1991; Oosterveld, 2003; Bluck et al., 2005). Diamonds were first discovered in Namibia in 1908 (near Luderitz) and in Namaqualand in 1925 (Port Nolloth area). Diamonds in Namaqualand have been recovered from fluvial and marine sediments extending from just south of the Olifants River, northwards to the Orange River (Fig. 1). In Namibia, economic quantities of diamonds occur in the region between the Orange River mouth and Luderitz, ~120 km to the north, although diamonds have been recovered as far north as the Hoanib River, ~1000 km from the Orange River mouth (Hallam, 1964).

Considerable controversy exists regarding the exact sources and depositional history of the West Coast diamonds. Although the immediate interiors of Namaqualand and Namibia host numerous alkaline intrusive bodies, none are diamond-bearing (e.g., Moore and Verwoerd, 1985; Kurszlaukis et al., 1998). The nearest known primary diamond occurrences are located more than 700 km to the east, on the Archaean Kalahari Craton (Fig. 1), which hosts more than 1000 kimberlites (also known as Group I or 'basaltic' kimberlites; e.g. Smith, 1983) and orangeites (also known as Group II or micaeous kimberlites; Smith, 1983), ranging in age from ~80 to ~1350 Ma (Table 1). Most researchers have suggested that the West Coast diamonds originated from erosion of kimberlites and orangeites located on the Kaapvaal Craton, with diamonds transported to the coast by the paleo-Orange River (Fig. 1) (e.g., de Wit 1999; de Wit et al., 1999; Bluck et al., 2005 and references therein). However, others have argued that a large proportion of the West Coast diamonds were eroded from the more proximal Permo-Carboniferous (ca. 300 Ma) Dwyka Group glacial deposits (Fig. 1), with their ultimate source being pre-Karoo kimberlites in the interior of the Kalahari Craton (e.g.,

Sutherland, 1982; Van Wyk and Pienaar, 1986; Maree, 1987, 1988; Moore and Moore, 2004). Resolution of this controversy has important implications, not only for determining the source(s) of the West Coast diamond deposits, but also for reconstructing the paleo-drainage and landscape history of the region and realising the potential for undiscovered diamond-bearing kimberlites and/or orangeites beneath the Karoo Basin (Fig. 1).

In a previous study, Phillips and Harris (2009) described a novel approach for constraining the provenance of the Namibian diamond placer using $^{40}Ar/^{39}Ar$ ages determined on clinopyroxene inclusions extracted from detrital diamonds. Here, we utilise the same methodology to constrain the provenance and transport history of the Namaqualand diamond placer deposit. This approach is based on earlier $^{40}Ar/^{39}Ar$ studies of clinopyroxene inclusions in diamonds from kimberlites of known age, where the original intent was to determine diamond genesis ages (Phillips et al., 1989; Burgess et al., 1989, 1992). Analyses of clinopyroxene inclusions extracted (or exposed at surface) from Orapa (ca. 90 Ma), Jwaneng (ca. 240 Ma) and Premier (ca.1200 Ma) diamonds yielded ages approaching the times of kimberlite eruption (Phillips et al., 1991, 2004a; Burgess et al., 1992, 2004; Phillips and Harris, 2008); rather than diamond genesis events (ca.1.0 – 3.5 Ga; see Shirey et al. 2013 and references therein). This unexpected outcome is attributed to diffusion of radiogenic ^{40}Ar ($^{40}Ar^*$) to the diamond/inclusion interface zone during mantle residence at high temperatures and loss of this component during inclusion extraction (e.g., Phillips and Harris, 2004) (Fig. 2). These results raised the prospect of using $^{40}Ar/^{39}Ar$ dating of clinopyroxene inclusions as a tool to constrain the ages of source kimberlite (Phillips and Harris, 2008, 2009). The approach is, however, not entirely straightforward; despite some inclusions giving host kimberlite emplacement ages, others are characterised by older apparent ages (Phillips and Harris, 2008). The reason(s) for this behaviour is not fully understood, but may be due to partial retention of pre-eruption mantle $^{40}Ar^*$ in defect structures in the clinopyroxene inclusions (Phillips et al. 2004a; Phillips and Harris, 2008). Notwithstanding this complication, experiments on

clinopyroxene-bearing diamonds from the Orapa kimberlite showed that a significant proportion (35%) exhibit host emplacement kimberlite ages, with the majority (92%) giving $^{40}Ar/^{39}Ar$ ages within 100 Ma of kimberlite emplacement. Therefore, although the inclusion ages must be viewed strictly as maximum estimates for the age of the source kimberlites (or orangeites), the results still provide useful constraints on the provenance of detrital diamond deposits, particularly when used in conjunction with paleo-drainage reconstructions and diamond size distribution data (see Phillips and Harris, 2009).

In their study of clinopyroxene inclusions from Namibian detrital diamonds (n = 52), Phillips and Harris (2009) concluded that most diamonds were sourced from post-Karoo kimberlites and orangeites on the Kaapvaal Craton, with only minor contributions possible from older kimberlites and the Dwyka conglomerates and tillites. However, these results were too imprecise to ascertain whether the diamonds were sourced from ca.80-90 Ma kimberlites, ca.115-200 Ma orangeites, or both groups. In the current study, we analysed clinopyroxene inclusions extracted from a suite of detrital diamonds (n = 84) from the Namaqualand West Coast, using both traditional single-collector $^{40}Ar/^{39}Ar$ mass spectrometry and a new generation multi-collector mass spectrometer. The results obtained provide unprecedented insights into the provenance and transport history of these diamonds.

Geological Setting

Regional Geology

The interior of southern Africa is dominated by the Precambrian Kalahari Craton, which includes the Archaean Kaapvaal and Zimbabwe Cratons (Fig. 1), the Archaean-Paleoproterozoic Limpopo Mobile Belt (de Wit et al., 1992), and a series of flanking

Paleoproterozoic (Magondi, Okwa, Kheis belts, Rehoboth Sub-province) to Mesoproterozoic (Namaqua-Natal-Maud-Mozambique mobile belts) mobile belts (e.g., Thomas et al., 1994; Hanson et al., 2006; Jacobs et al., 2008). Rocks of the Phanerozoic Karoo Supergroup cover large areas of southern and central Africa, including much of the Kaapvaal craton (see review by Catuneanu et al., 2005 and references therein) (Fig. 1). The Dwyka Group forms the basal unit and is dominated by ca. 300 Ma glacial deposits (e.g. Visser, 1997; Bangert et al., 1999). In the southern African Karoo basin, the Dwyka Group is overlain by the sediment-dominated Permian Ecca and Permo-Triassic Beaufort Groups (e.g. SACS, 1980; Johnson et al., 1997) and the Triassic-Jurassic Stormberg Group, which includes the ca. 180 Ma Drakensberg flood basalt province (e.g., Duncan et al., 1997; Jourdan et al., 2007).

Southern Africa has experienced widespread alkaline magmatism over much of its geological history (e.g., Hanson et al., 2006), including the emplacement of archetypal kimberlite (also known as Group I kimberlites) and orangeite (also known as Group II or micaceous kimberlites) pipes, dykes and sills (e.g., Jelsma et al., 2004). Diamondiferous localities are, however, confined almost exclusively to the Kaapvaal Craton, Zimbabwe Craton and Limpopo Belt (Azanian Craton; McCourt et al., 2004). Known kimberlite and orangeite localities were emplaced over a broad time period, from ca. 60 to 1600 Ma (e.g., Allsopp et al., 1989; Jelsma et al., 2004; Gurney et al., 2005), with the major epochs summarised in Table 1. Pre-Karoo diamondiferous localities include ca. 500 Ma kimberlites in northern South Africa (e.g., Marnitz, Venetia) and Zimbabwe (e.g., Beit Bridge, Colossus) (Phillips et al., 1999), the ~1.2 Ga Premier kimberlite cluster in north-central South Africa (Kramers and Smith, 1983), and the ca.1.35 Ga Martins Drift kimberlites in eastern Botswana (Jelsma et al., 2004). Alluvial diamonds recovered from the ca.2.7-3.1 Ga Witwatersrand Basin imply even older diamondiferous kimberlites or related rocks in the region (e.g. Smart et al., 2016). Known syn-Karoo diamondiferous bodies are restricted to the Jwaneng kimberlite cluster (ca. 240 Ma) in southern Botswana (Kinny et al., 1989; Phillips et al.,

2004a). Post-Karoo Cretaceous (~80 – 95 Ma) kimberlites and Cretaceous/Jurassic (~110 - ~200 Ma) orangeites are by far the most abundant and widespread of the groups (Fig. 1), with the orangeites showing a distinct age progression across the Kalahari Craton from Dokolwayo (ca. 200 Ma) in Swaziland to Sutherland (ca. 110 Ma) in the southern Cape (Table 1).

The current drainage system in southern Africa is dominated by the Orange-Vaal River basin, which also includes the Harts, Molopo and Fish River tributaries. This basin drains an area of approximately 1x106 km^2, and encompasses much of the hinterland (Dingle and Hendy, 1984). This system covers large areas of the Kalahari Craton that hosts the diamond-bearing kimberlites and orangeites described above (Table 1).

Namaqualand diamond placer deposits

Diamond placer deposits in Namaqualand extend from just south of the Olifants River to the mouth of the Orange River, a distance of some 400 km (e.g. Hallam, 1964; Bluck et al., 2005) (Fig. 1). The main deposits, which occupy a coastal region of a few kilometres width, occur as a complex succession of Oligocene to Holocene raised beach terrace gravels and river channel gravels, with lesser deposits off-shore (Hallam, 1964; Bluck et al., 2005). The beach terrace deposits formed in response to multiple regressions and transgressions imposed by fluctuations in relative sea-level (e.g., Bluck et al., 2005, 2007 and references therein).

Diamond size generally decreases northwards (Hallam, 1964; Sutherland, 1982), and this has been taken as evidence that the Olifants River may have been the major point source of diamonds to the Namaqualand Coast (e.g. Hallam, 1964; Bluck et al., 2005; cf. Moore and Moore, 2004). This is supported by the presence of Early Aptian to Cenomanian (93 – 112 Ma) deltaic sediments near the mouth of the current Olifants River (Dingle et al., 1983; Brown et al., 1995). However, other westward draining fluvial systems, such as the Buffels and Groen fluvial systems are associated with diamond-bearing terraces and likely contributed

at least some diamonds to the coastal deposits (Stevenson and McMillan, 2004). The northerly distribution of diamonds along the West Coast is attributed to the strong northerly-directed ocean currents, waves, winds and longshore drift, operating over a shallow coastal shelf in a semi-arid climatic environment (e.g., Bluck et al., 2005). These factors caused reworking of older beach deposits and concentration of diamonds northwards. Similarly, diamonds transported by the proto-Orange River have been reworked northwards along the Namibian Coast, with limited contributions to Namaqualand placer deposits (e.g., Bluck et al., 2005).

Sample Selection

A total of 84 detrital diamonds, containing clinopyroxene inclusions, were collected from run-of-mine Namaqualand productions by staff of the Geology Section of the Diamond Trading Company, RSA (Pty) Ltd, Kimberley (Table 2). The diamonds originate from onshore locations within the Keinzee and Koignaas licence areas between Hondeklipbaai and Port Nolloth (~80 – 200 km south of the Orange river mouth; Fig. 1). The diamonds are mostly pale yellow to pale brown with characteristic, variably resorbed, 'rounded dodecahedral' morphologies. All diamonds were examined under a binocular microscope to ensure that the inclusions were totally enclosed by diamond and free of alteration.

The clinopyroxene inclusions were released by individually crushing the host diamond in a steel anvil device (Fig. 3). Some inclusions were recovered intact, but, the majority broke into fragments in the range 100 – 300 μm in in length (Tables 2, 3). Several stones contained multiple inclusions, some of which were analysed separately (Tables 2, 3). All inclusions were characterised by imposed cubo-octahedral morphologies, indicating a syn-genetic origin with the host diamond (e.g., Harris, 1992). Clinopyroxene inclusions from the study were assigned to peridotitic or eclogitic parageneses based on colour; the former being characteristically emerald-green Cr-diopside and the latter being pale green in colour, with omphacitic

compositions (e.g., Meyer, 1987; Phillips et al., 2004). Inclusions from a small number of diamonds (n = 4) contained negligible potassium and may have been pale green enstatite inclusions.

Analytical Methods

Clinopyroxene inclusions, extracted from their host diamonds, were analysed in two separate batches, using different mass spectrometer systems. Batch A inclusions (NQ1 – NQ48) were analysed in 2008 (MM5400 mass spectrometer), with batch B (NQ100 – NQ135) inclusions analysed in 2016 (ARGUSVI multi-collector mass spectrometer). All inclusions were ultrasonically cleaned in de-ionised water and acetone and then individually wrapped in aluminium foil packets and placed in a quartz glass vial, together with interspersed aliquots of irradiation monitors. Batch A inclusions were packaged with aliquots of the irradiation monitor GA1550 biotite (99.125 ± 0.076 Ma; Phillips et al., 2017), plus packets of CaF_2 and K-glass to monitor contributions from interfering isotopes. These packages were irradiated in two cans (UM#2, 16 hrs; UM#3, 28 hrs), in position 5c of the McMaster University Research reactor, in Hamilton, Ontario. Packets of Batch B inclusions were interspersed with aliquants of the Fish Canyon Tuff (FCT) sanidine monitor (28.126 ± 0.019 Ma; Phillips et al., 2017) and irradiated in the CLICIT facility of the Oregon State University TRIGA (OSTR) reactor (UM#68; 100 hrs).

After irradiation and cooling, inclusions were loaded into copper sample trays, which were placed in vacuum ports and baked at ~120°C for 24 hours. $^{40}Ar/^{39}Ar$ analyses were conducted at the University of Melbourne. Analytical procedures for Batch A inclusions were analogous to those described by Phillips et al. (2004) and Phillips and Harris (2008). In this case, laser step-heating was achieved using a defocused Spectron Nd-YAG laser and argon isotopic analyses were carried out on a MM5400 mass spectrometer, equipped with a Daly

detector. Protocols for analysis of Batch B inclusions are described in Phillips & Matchan (2013) and Phillips et al. (2017). Here, $^{40}Ar/^{39}Ar$ analyses were carried out using a multi-collector Thermo Fisher Scientific ARGUSVI mass spectrometer linked to a stainless-steel gas purification line and a Photon Machines Fusions 10.6 CO_2 laser system.

$^{40}Ar/^{39}Ar$ results

$^{40}Ar/^{39}Ar$ step-heating and fusion results for clinopyroxene inclusions extracted from Batch A (NQ1 – NQ48) and Batch B (NQ100 – NX135) Namaqualand detrital diamonds are summarised in Tables 2 and 3. Detailed $^{40}Ar/^{39}Ar$ analytical data are tabulated in tables A1 and A2 (electronic appendix). Ages were calculated using the atmospheric argon composition of Lee et al. (2006) and the decay constants of Steiger and Jäger (1977). Unless otherwise stated, errors are listed with two sigma (2σ) uncertainties.

In most cases, larger inclusion fragments from individual diamonds were combined in two- to three-step heating experiments, whereas smaller inclusion fragments were fused in single-step analyses. Three diamonds (NQ9, NQ26, NQ101) contained sufficiently large inclusions to analyse two aliquots in separate step-heating experiments. Weights of clinopyroxene inclusions from each diamond were estimated using measured dimensions of inclusion fragments (assuming a density of 3.3 $g.cm^{-3}$) and from Ca/K ratios calculated from $^{40}Ar/^{39}Ar$ step-heating data (see Burgess et al., 1992 for calculation details). For inclusions confirmed as clinopyroxene, uncertainties associated with these calculations are estimated at ca. ~30%. Results from the two methods are broadly concordant, although the dimensional calculations give consistently larger inclusion weights (Table 2). Aliquot weights for Batch A and B inclusions range from 2 to 508 μg and 3 to 248 μg, respectively (Table 2).

Potassium contents were estimated from Ca/K ratios determined from argon isotopic analyses (Table A1) and assumed Ca contents for clinopyroxene (10 wt.% Ca in eclogitic and

14 wt.% Ca in peridotitic clinopyroxene, respectively; see Phillips et al., 2004a for details). Estimated potassium contents for Batch A inclusions vary from 46 ppm to 14,436 ppm, with a mean value of 2643 ppm (Table 2). Batch B inclusions exhibit potassium levels of 155 ppm to 6302 ppm, with a mean value of 2749 ppm (Table 2). There are no systematic differences in K content between peridotitic and eclogitic inclusions. These values are analogous to those determined from previous $^{40}Ar/^{39}Ar$ studies of clinopyroxene inclusions in diamonds (e.g. Burgess et al., 1992; Phillips et al., 2004a; Phillips and Harris, 2008; Laiginhas et al., 2008) and are also consistent with electron microprobe data for clinopyroxene inclusions from a study of Namibian detrital diamonds (249-3000 ppm K; average = 1879 ppm; Loest et al., 2003). Inclusions from three Batch A and one Batch B diamonds yielded negligible $^{39}Ar_K$, suggesting that they were not clinopyroxene, but rather pale green enstatite (Table 2).

The multi-collector ARGUSVI (Batch B) results are significantly more precise (>10x) than those determined using the older generation MM5400 system (Batch A). This is due to a combination of improved pre-treatment routines (low temperature laser heating), which reduced atmospheric contamination and increased radiogenic $^{40}Ar^*$ yields, and high precision multi-collection analyses (see Phillips and Matchan, 2013 and Phillips et al., 2017 for more details). In general, the larger, more potassium-rich inclusions yielded more robust age results (Table 2). Several smaller and/or potassium-poor inclusions produced insufficient $^{39}Ar_K$ or $^{40}Ar^*$ for accurate age determination and only those age results with uncertainties of <50% are plotted in Figure 4. With one exception (NQ109), low temperature steps exhibit older apparent ages than high temperature steps (Table A1). This is attributed to retention of small quantities of pre-eruption ^{40}Ar within the inclusion during the diamond's residence in the mantle. Alternative explanations, such as recoil loss of $^{39}Ar_K$ (i.e. ^{39}Ar ejected from inclusion margins during neutron irradiation with an average recoil distance of ~0.1μm; Turner and Cadogan, 1974), are not consistent with the non-systematic variations in $^{40}Ar^*/^{39}Ar$ ratios and/or the relatively large size of the inclusions. NQ109 is the only inclusion analysed that yielded a low-temperature

apparent age (120.6 ± 15.5 Ma) that is distinctly younger than the fusion age (227.7 ± 7.0 Ma); reasons for this anomaly are unclear. As the inclusion ages are considered to be maximum estimates for the time of the host magma eruption, the youngest ages (i.e., high-temperature fusion steps) provide the closest approximation for the timing of source kimberlite/ orangeite emplacement (see Phillips and Harris, 2009).

Of the Batch A inclusion aliquots analysed, 33 of 48 yielded ages with uncertainties <50% (Table 3), and apparent ages ranging from 117.5 ± 43.6 Ma to 3684 ± 191 Ma (2σ) (Fig. 4a). Six inclusions (18%) have ages that are within error of, or older than 300 Ma (Dwyka Group deposition age) and five inclusions (15%) are older than 500 Ma (Fig. 4a). The majority (31 of 36) of Batch B inclusion aliquots yielded sufficient $^{39}Ar_K$ for reliable age determination, with values ranging from 120.6 ± 15.4 Ma to 688.8 ± 4.9 Ma (2σ) (Table 3). Of these, 7 of 31 exhibit apparent ages within error, or older than 300 Ma, whereas only two inclusions display ages older than 500 Ma (Fig. 4b; Table 3). As expected for multi-collector ARGUSVI data, the Batch B data are characterised by significantly smaller uncertainties than the Batch A results.

Where argon yields were significant, inclusion aliquots generally yielded analogous Ca/K ratios for low and high temperature steps, indicating homogeneous compositions (Table 3). The few inclusions with more diverse Ca/K values may result from the presence of additional intergrowth phases (e.g., garnet; Phillips et al., 2004b). There are no obvious correlations between apparent ages and sample weights, potassium contents, Ca/K ratios or inclusion paragenesis (Table 3).

In summary, it is noteworthy that all Batch B ages are distinctly older than 100 Ma, with most ages in the interval 100 – 300 Ma (Fig. 4b). Similarly, none of the Batch A inclusions yielded absolute ages younger than 100 Ma, although four aliquots have relatively large uncertainties that extend to less than 100 Ma (Fig. 4a).

Discussion

$^{40}Ar/^{39}Ar$ clinopyroxene inclusion ages

The two batches of clinopyroxene inclusions from Namaqualand diamonds yielded similar apparent age distributions, with overall apparent ages ranging from 117 ± 39 Ma to 3.8 ± 0.2 Ga (Table 2). As noted above, previous $^{40}Ar/^{39}Ar$ studies of clinopyroxene inclusions in diamonds from kimberlites of known age (i.e. ca.90 Ma Orapa, ca.240 Ma Jwaneng, ca.1200 Ma Premier kimberlites) demonstrated that up to 100% of the $^{40}Ar^*$ produced in the mantle prior to host emplacement is lost during inclusion extraction (Fig. 2; Phillips et al., 1989; Phillips et al., 2004a; Phillips and Harris, 2008). However, as many inclusions retain some proportion of the pre-emplacement $^{40}Ar^*$ (possibly in defect sites), the inclusion ages must be considered maximum estimates of host kimberlite/orangeite emplacement. At the same time, the Orapa study showed that most extracted inclusions have lost >90% of their pre-emplacement $^{40}Ar^*$, assuming diamond formation ages of >1.1 Ga (e.g., Richardson et al., 1999, 2001).

Constraints on diamond provenance

As summarised in Table 1, known diamondiferous kimberlites in the Namaqualand hinterland range in age from ca.80 to 1350 Ma, with distinct peaks in activity at ca.80-90 Ma, ca.240 Ma, ca.500 Ma, ca.1200 Ma and ca.1350 Ma (see summary by Jelsma et al., 2008). In contrast, diamond-bearing orangeites are limited to the interval 115 – 200 Ma (Table 1; Jelsma et al., 2008). Pre-Dwyka kimberlites are all older than ca.500 Ma, with post-Dwyka kimberlites restricted to the ca.80-90 Ma and ca.240 Ma kimberlite clusters.

The majority of Namaqualand clinopyroxene inclusion ages (>90%) are younger than 500 Ma (the youngest known pre-Karoo kimberlites) (Tables 2, 3). Being maximum age

constraints, the current results indicate that the vast majority of Namaqualand diamonds were sourced from post-Dwyka kimberlites and/or orangeites (Fig. 1); these include the ca.80-90 Ma group of kimberlites, the ca.115-200 Ma orangeites and the ca.240 Ma Jwaneng kimberlite cluster (Table 1). This finding accords with previous age results for clinopyroxene-bearing diamonds from the Namibian placer deposit north of the Orange River (Phillips and Harris, 2009). Therefore, these data do not support suggestions that significant quantities of detrital diamonds in the Namibian and Namaqualand deposits originate from erosion of secondary sedimentary sources such as the ca. 300 Ma Dwyka tillite deposits and/or older West Coast sedimentary successions, such as the Nama and Cape Supergroups (e.g., Moore and Moore, 2004).

There are, however, subtle differences in age distributions between the Namibian and Namaqualand clinopyroxene inclusions. Approximately 31% (14 of 45) of Namibian inclusions produced ages within error of ca.80-90 Ma kimberlites (Phillips and Harris, 2009). Although ~18% (8 of 45) of these ages are also within 2σ-uncertainty of the youngest diamond-bearing orangeites (ca.115 Ma), 13% (6 of 45) have smaller uncertainties and can only be derived from the ca.80-90 Ma kimberlites. Based on a direct comparison between the Orapa and Namibian clinopyroxene age distributions, Phillips and Harris (2009) suggested that the Namibian detrital deposit includes roughly equal proportions of diamonds from ca.80-90 Ma kimberlites and ca.115-200 Ma orangeites. In contrast to the Namibian inclusion ages, only three of the Batch A Namaqualand inclusion ages are within 2σ-uncertainty of 90 Ma; and none can be assigned unequivocally to the 80-90 Ma age group. The higher precision Batch B results are more definitive, with no ages within error of 90 Ma. Although we cannot rule out the possibility of ca.80-90 Ma kimberlites contributing to the Namaqualand diamonds, this analysis suggests that most Namaqualand diamonds were instead eroded from slightly older primary sources, with the ca.115-200 Ma orangeites being the most likely candidates.

Notwithstanding the above arguments, it is still possible that a small proportion of diamonds may have originated from pre-Dwyka kimberlites (or undiscovered orangeites). Known pre-Karoo diamond-bearing kimberlites in southern Africa include the ca.500 Ma Marnitz, Venetia, Murowa and Colossus kimberlites in northern South Africa and Zimbabwe, the ca.1.2 Ga Premier cluster near Cullinan, South Africa, and the ca.1.35 Ga Martin's Drift kimberlites in eastern Botswana (Table 1). Taking account of the large uncertainties associated with some inclusion ages, Phillips and Harris (2009) concluded that <5% (2 of 45) of ages from Namibian inclusions are within error, or older than 500 Ma. This is analogous to the small proportion (9%) of Namaqualand inclusion ages ≥500 Ma (Tables 2, 3). Therefore, it is feasible that ≥500 Ma kimberlites contributed a small fraction (<10%) of West Coast detrital diamonds, either transported to the West Coast directly, or via secondary sedimentary sources such as the Dwyka tillite. It is also possible that a very minor fraction of the diamonds (one of 84; 1%) could have been reworked from the ca.2.7-3.1 Ga Witwatersrand Basin (e.g., Smart et al., 2016). However, a small proportion of clinopyroxene inclusions from Orapa and Jwaneng diamonds (where eruption ages are known) exhibit apparent ages up to 1.0 Ga older than the time of host emplacement (Phillips et al., 2004a, Phillips and Harris, 2008); therefore, it is equally likely that the elevated apparent ages simply reflect greater retention of pre-eruption argon in the diamonds.

Paleo-drainage constraints on diamond transport

A number of paleo-drainage reconstructions have been proposed for the post-Gondwanan evolution of southern Africa's river systems. For example, Dingle and Hendey (1984) suggested that the post-Gondwana Orange River initially established its conduit to the Atlantic Ocean, before switching to a more southerly outlet close to the current Olifants River mouth during the Paleogene, and then returning to its current position in the Neogene. More recent studies have

favoured the early establishment of two separate River systems in the Late Cretaceous, a northerly 'Kalahari' River that followed a course similar to the current Molopo River with an outlet near the modern Orange River, and a 'Karoo' River to the south, which drained the interior of the Kaapvaal craton and flowed into the Atlantic adjacent to the current Olifants River mouth (Fig. 5a) (e.g., Partridge, 1998; de Wit, 1993, 1999; de Wit et al., 2000). De Wit (1993, 1999) suggested that the Karoo River was then captured by the Kalahari River to establish the current Orange River system during the Neogene. However, studies of the off-shore sequence stratigraphy along the Atlantic coast show the presence of two significant paleo-deltas associated with the precursor Orange (ca.70-93 Ma) and Olifants River deltas (ca.93-112 Ma) (e.g., Brown et al., 1995; Aizawa et al., 2000). Given the difference in delta formation ages, Bluck et al. (2005) suggested that the Karoo River only persisted to the Late Cretaceous and that the modern Orange River drainage system was established by ca.95 Ma and has remained largely unchanged since this time (e.g., Ward and Bluck, 1997) (Fig. 5b). The latter scenario is consistent with thermochronological constraints on regional denudation events (e.g., Gallagher and Brown, 1999; Brown et al., 1999) and implies that the Namaqualand diamonds were eroded from sources such as the ca.115-200 Ma orangeites and older kimberlites, to the exclusion of the 80-90 Ma kimberlites (Bluck et al., 2005).

Formation of the Namaqualand and Namibian diamond placers

The combined evidence from the $^{40}Ar/^{39}Ar$ inclusion results, paleo-drainage reconstructions and diamond size distribution data permit the development of a comprehensive model for the formation and evolution of the Namaqualand and Namibian detrital diamond deposits. The available data indicate that the vast majority of Namaqualand diamonds were likely sourced from Early Cretaceous to Jurassic orangeites located on the Kaapvaal Craton. These diamonds were transported to the West Coast by the Early Cretaceous Karoo River with its outlet close to

410 the modern Olifants River (Fig. 5a). Prevailing north-directed ocean currents then reworked the
411 diamonds northwards along the Namaqualand coast, forming successive beach terraces and
412 alluvial deposits in response to relative sea-level fluctuations. Smaller local Rivers draining the
413 interior of Namaqualand may also have reworked earlier alluvial deposits, thereby establishing
414 local diamond sub-populations and size distributions (e.g. Bluck et al., 2005). Assuming that
415 the inclusion-bearing diamonds analysed in this study are representative of the Namaqualand
416 diamond population as a whole, contributions from the Dwyka Group sediments and, hence
417 older kimberlites, were minimal.

418 As described by Phillips and Harris (2009), the $^{40}Ar/^{39}Ar$ inclusion data and paleo-
419 drainage patterns indicate that the Namibian diamond deposit probably formed subsequent to
420 establishment of the 'modern' Orange River drainage in the Late Cretaceous (post ~95 Ma).
421 Widespread drainage of the Kaapvaal Craton likely sourced the majority of diamonds from 80-
422 90 Ma kimberlites, with additional contributions from already partially eroded ca.115-200 Ma
423 orangeites. After transport of the diamonds to the coast by the Orange River drainage system,
424 the diamonds were reworked into successively younger beach terraces and River gravels along
425 the Namibian Coast and lower Orange River, respectively (e.g. Bluck et al., 2005). It is also
426 possible that capture of the Karoo River by the Orange River drainage might have reworked
427 earlier orangeite diamonds along the proposed Koa River (e.g., de Wit, 1999).

428 Finally, the purported Kalahari River is thought to have drained areas of southern
429 Botswana (e.g., de Wit, 1999). Therefore, it is possible that diamonds from the Jwaneng
430 kimberlite cluster might were also transferred to the Namibian placer deposit and reworked into
431 younger beach deposits. However, it is not possible to distinguish this age population with
432 confidence from the available $^{40}Ar/^{39}Ar$ inclusion data as ages approaching ca.240 Ma could
433 also result from pre-eruption $^{40}Ar^*$ retained in diamonds from younger orangeites and
434 kimberlites (Table 2).

435

Conclusions

Two batches of clinopyroxene inclusions extracted from Namaqualand detrital diamonds exhibit apparent ages consistent with the derivation of most diamonds (>85%) from ca.115-200 Ma orangeites located on the Kaapvaal Craton. Therefore, few, if any Namaqualand diamonds are likely to be eroded from the ca.300 Ma Dwyka tillites and, hence, older kimberlites. Paleo-drainage reconstructions support transport of the diamonds to the Namaqualand Coast by the 'paleo-Karoo' River. Capture of this River system by the 'paleo-Kalahari' River in the Late Cretaceous, to the form modern Orange River system, facilitated formation of the Namibian diamond placer, with diamonds sourced from Cretaceous-Jurassic kimberlites and orangeites on the Kaapvaal Craton.

Acknowledgements We are indebted to the De Beers Group for donation of the Namaqualand diamonds, logistical and financial support, and permission to publish. We are especially indebted to V.G. Anderson, J. Parker and E. van Blerk, of Harry Oppenheimer House in Kimberley, for selection of clinopyroxene-bearing diamonds. We thank S. Szczepanski for technical assistance with the $^{40}Ar/^{39}Ar$ analyses. We acknowledge the constructive comments by the two reviewers (S. Shirey and R. Burgess) of the manuscript, and the editorial handling of T. Stachel.

References

Aizawa M, Bluck BJ, Cartwright J, Milner S, Swart R, Ward, JD (2000) Constraints on the geomorphological evolution of Namibia from the offshore stratigraphic record. Geol Surv Namibia, Heno Martin vol 12, pp 337–346

461 Allsopp, HL, Barrett, DR (1975) Rb-Sr age determinations on South African kimberlite pipes.
462 Phys Chem Earth 9:605–618
463 Allsopp HL, Roddick JC, (1985) Rb-Sr and ^{40}Ar-^{39}Ar age determinations on phlogopite micas
464 from the pre-Lebombo Group Dokolwayo pipe. Geol Soc S Afr, Spec Publ 13:267–
465 271
466 Allsopp HL, Bristow JW, Smith CB, Brown R, Gleadow AJW, Kramers JD, Garvie OG
467 (1989) A summary of radiometric dating methods applicable to kimberlites and related
468 rocks. In: Ross J (ed) Kimberlites and Related Rocks, vol 1. Geol Soc Austr, Spec
469 Publ 14, pp 343–357
470 Ayres NP, Hatton CJ, Quadling KE, Smith CB (1998) Update on the distribution in time and
471 space of southern African kimberlites. De Beers Geoscience Centre, Johannesburg, 1:5
472 000 000 poster.
473 Bangert B, Stollhofen H, Lorenz V, Armstrong RA (1999) The geochronology and
474 significance of ash-fall tuffs in the glaciogenic Carboniferous-Permian Dwyka Group
475 of Namibia and South Africa. J Afr Earth Sci 29:33–49
476 Bluck BJ, Ward JD, de Wit MCJ (2005) Diamond mega-placers: southern Africa and the
477 Kaapvaal craton in a global context. In: McDonald I, Boyce AJ, Butler IB, Herrington
478 RJ, Polya DA (eds) Mineral Deposits and Earth Evolution. Geol Soc Lond Spec Publ
479 248, pp 213–245
480 Bluck BJ, Ward JD, Cartwright J, Swart R (2007) The Orange River, southern Africa: an
481 extreme example of a wave-dominated sediment dispersal system in the South Atlantic
482 Ocean. J Geol Soc Lond 164:341–351
483 Brown LF, Benson JM, Brink GJ, Doherty S, Jollands, A, Jungslager, EHA, Keenan, JHG,
484 Muntingh, A, Van Wyk, NJS (1995) Sequence stratigraphy in offshore South African
485 divergent basins. An Atlas for exploration of Cretaceous low stand traps by Soekor
486 (Pty) Ltd. Am Assoc Petrol Geologists. Studies in Geology 41, 184p

Brown RW, Gallagher K, Gleadow AJ, Summerfield M (1999) Morphotectonic evolution of the South Atlantic margins of Africa and South America. In: Summerfield, M.A. (Ed.), Geomorphology and global tectonics. John Wiley & Sons Ltd: pp. 255–281.

Burgess R, Turner G, Laurenzi M, Harris JW (1989) $^{40}Ar/^{39}Ar$ laser probe dating of individual clinopyroxene inclusions in Premier eclogitic diamonds. Earth Planet. Sci. Lett. 94, 22–28.

Burgess R, Turner G, Harris JW (1992) $^{40}Ar/^{39}Ar$ laser probe studies of clinopyroxene inclusions in eclogitic diamonds. Geochim Cosmochim Acta 56:389–402

Burgess R, Kiviets GB, Harris JW (2004) Ar-Ar age determinations of eclogitic clinopyroxene and garnet inclusions in diamonds from the Venetia and Orapa kimberlites. Lithos 77:113–124

Catuneanu O, Wopfner H, Eriksson PG, Cairncross B, Rubidge BS, Smith RMH, Hancox PJ (2005) The Karoo basins of south-central Africa. J Afr Earth Sci 43:211–253

Davis GL (1977) The ages and uranium contents of zircons from kimberlites and associated rocks. Carnegie Inst Wash Yearbook 76:631–635

de Wit MCJ (1999) Post-Gondwana drainage and the development of diamond placers in western South Africa. Econ Geol 94:721–740

de Wit MJ, de Ronde CEJ, Tredoux M, Roering C, Hart RJ, Armstrong RA, Green RWE, Peberdy E, Hart RA (1992) Formation of an Archean continent. Nature 357:553–562

Dingle RV, Hendy QB (1984) Late Mesozoic and Tertiary sediment supply to the Eastern Cape basins (SE Atlantic) and the palaeo-drainage systems in southwestern Africa. Marine Geol 56:13–26

Duncan RA, Hooper PR, Rehacek J, Marsh JS, Duncan AR (1997) The timing and duration of the Karoo igneous event, southern Gondwana. J Geophys Res 102:18127–18138

Gallegher K, Brown R, (1999) Denudation and uplift at passive margins: the record on the Atlantic Margin of southern Africa. Phil Trans R Soc Lond A357: 835–859.

513 Gurney JJ, Helmstaedt HH, Le Roux AP, Nowicki TE, Richardson SH, Westerlund KJ (2005)
514 Diamonds: Crustal distribution and formation processes through time and space and an
515 integrated deposit model. In: Hedenquist JW, Thompson JFH, Goldfarb RJ, Richards
516 JP (eds) Econ Geol 100:143–177
517 Hanson RE, Harmer RE, Blenkinsop TG, Bullen DS, Dalziel IWD, Gose WA, Hall RP,
518 Kampunzu AB, Key RM, Mukwakwami J, Munyanyiwa H, Pancake JA, Seidel EK,
519 Ward SE (2006) Mesoproterozoic magmatic and tectonic evolution in the Kalahari
520 Craton. J Afr Earth Sci 46:141–167
521 Hallam CD (1964) The geology of the coast diamond deposits of southern Africa. In:
522 Haughton SH (ed) The Geology of some Ore Deposits in Southern Africa. Geol Soc
523 South Afr 2:671–728
524 Harris JW (1992) Diamond Geology. In: Field JE (ed) The Properties of Natural and
525 Synthetic Diamonds. Academic Press, London, pp 345-393
526 Hartnady C, Joubert P, Stowe C (1985) Proterozoic crustal evolution in southwestern Africa.
527 Episodes 8:236–244
528 Jacobs J, Pisarevsky S, Thomas RJ, Becker T (2008) The Kalahari Craton during assembly
529 and dispersal of Rodinia. Precam Res 160:142–158
530 Jelsma HA, de Wit MJ, Thiart C, Dirks PHGM, Viola G, Basson IJ, Anckar E (2004)
531 Preferential distribution along transcontinental corridors of kimberlites and related
532 rocks of Southern Africa. S Afr J Geol 107:301–324
533 Johnson MR, van Vuuren CJ, Visser JNJ, Cole DJ, Wickens HdeV, Christie ADM, Roberts
534 DL (1997) The foreland Karoo Basin, South Africa. In: Selley RC (ed) African Basins
535 – Sedimentary Basins of the World. Elsevier, Amsterdam, pp 269–317
536 Jourdan F, Feraud G, Bertrand H, Watkeys MK, Renne PR (2007) Distinct brief major events
537 in the Karoo large igneous province clarified by new $^{40}Ar/^{39}Ar$ ages on the Lesotho
538 basalts. Lithos 98:195–209

Kinny PD, Compston W, Bristow JW, Williams IS (1989) Archaean mantle xenocrysts in a Permian kimberlite: Two generations of kimberlitic zircon in Jwaneng DK2, southern Botswana. In: Ross J (ed) Kimberlites and related rocks. Geol Soc Austr Spec Publ 14, pp 833-842

Kramers JD, Smith CB (1983) A feasibility study of U-Pb and Pb-Pb dating of kimberlites using groundmass mineral fractions and whole rock samples. Isot Geosci 1:23–38

Kurszlaukis S, Franz L, Lorenz V (1998) On the volcanology of the Gibeon kimberlite field, Namibia. J. Volcanol Geotherm Res 84:257–272

Laiginhas F, Pearson DG, Phillips D, Burgess R, Harris JW (2008) Re-Os and Ar-Ar isotope measurements of inclusions in diamonds from the Ural Mountains: constraints on diamond genesis and eruption ages. 9th Int Kimberlite Conf, Frankfurt, Extd abstr, 9IKC-A-00147

Loest I, Stachel T, Brey GP, Harris JW, Rybchikov ID (2003) Diamond formation and source carbonation: mineral associations in diamonds from Namibia. Contrib Mineral Petrol 145:15–24

Maree BD (1987) Die afsetting en verspreiding van spoeldiamante in Suid-Afrika. S Afr J Geol 90:428–447

Meyer HOA (1987) Inclusions in diamond. In: Nixon PH (ed) Mantle Xenoliths. John Wiley & Sons, Chichester, pp 501–522

Moore JM, Moore AE (2004) The roles of primary kimberlitic and secondary Dwyka glacial sources in the development of alluvial and marine diamond deposits in Southern Africa. J Afr Earth Sci 38:115–134

Moore JM, Verwoerd WJ (1985) The olvine melilitite-“kimberlite”-carbonatite suite of Namaqualand and Bushmanland, South Africa. Trans Geol Soc S Afr 88:281–294

Oosterveld MM (2003) Evaluation of alluvial diamond deposits Alluvial diamonds in South Africa. Geol Soc S Afr workshop, pp 1–7

565 Phillips D (1991) Argon and halogen chemistry of phlogopite from South African kimberlites:
566 a combined step-heating, laser probe, electron microprobe and TEM study. Isot Geosci
567 87:71–98
568 Phillips D, Onstott TC, Harris J W (1989) $^{40}Ar/^{39}Ar$ laser probe dating of diamond inclusions
569 from the Premier kimberlite. Nature 346: 54–56
570 Phillips D, Machin KJ, Kiviets GB, Fourie LF, Roberts MA, Skinner EMW (1998) A
571 petrographic and $^{40}Ar/^{39}Ar$ geochronological study of the Voorspoed kimberlite, South
572 Africa: Implications for the origin of Group II kimberlite magmatism. S Afr J Geol
573 101:299–306
574 Phillips D, Kiviets GB, Barton ES, Smith CB, Viljoen KS, Fourie LF (1999) $^{40}Ar/^{39}Ar$ dating
575 of kimberlites and related rocks: problems and solutions. In: Gurney JJ, Gurney JL,
576 Pascoe MD, Richardson SH (eds) Proc 7th Int Kimberlite Conf, The PH Nixon Vol,
577 pp 677–688
578 Phillips D, Harris JW, Kiviets GB (2004a) $^{40}Ar/^{39}Ar$ analyses of clinopyroxene inclusions in
579 African diamonds: implications for source ages of detrital diamonds. Geochim
580 Cosmochim Acta 68:151–168
581 Phillips D, Harris JW, Viljoen KS (2004b) Mineral chemistry and thermobarometry of
582 inclusions from the Be Beers Pool diamonds, Kimberley, South Africa. Lithos 77:155–
583 179
584 Phillips D, Harris JW (2008) Provenance studies from $^{40}Ar/^{39}Ar$ dating of mineral inclusions
585 in diamonds: Methodological tests on the Orapa kimberlite, Botswana. Earth Planet
586 Sci Lett 274:169–178
587 Phillips D, Harris JW (2009) Diamond provenance studies from $^{40}Ar/^{39}Ar$ dating of
588 clinopyroxene inclusions: An example from the west coast of Namibia. Lithos
589 S112:794–805

590 Phillips D, Matchan E (2013) Ultra-high precision $^{40}Ar/^{39}Ar$ ages for Fish Canyon Tuff and
591 Alder Creek Rhyolite sanidine: new dating standards required? Geochim
592 Cosmochimica Acta, 121, 229-239
593 Phillips D, Matchan EL, Honda M, Kuiper KF (2017). Astronomical calibration of $^{40}Ar/^{39}Ar$
594 reference minerals using high-precision, multi-collector (ARGUSVI) mass
595 spectrometry. Geochim Cosmochim Acta 196:351–369
596 Richardson SH, Chinn IL, Harris JW (1999) Age and origin of eclogitic diamonds from the
597 Jwaneng kimberlite, Botswana. In: Gurney JJ, Gurney JL, Pascoe MD, Richardson SH
598 (eds) Proc 7th Int Kimberlite Conf. The PH Nixon vol, pp 709–713
599 Richardson SH, Shirey SB, Harris JW, Carlson RW (2001) Archean subduction recorded by
600 Re-Os isotopes in eclogitic sulfide inclusions in Kimberley diamonds. Earth Planet Sci
601 Lett 191:257–266
602 Shirey SB, Cartigny P, Frost DJ, Keshav S, Nestola F, Nimis P, Pearson DG, Sobolev NV,
603 Walter MJ (2013) Diamonds and the Geology of Mantle Carbon. Rev Minerol
604 Geochem 75: 355-421
605 Smart KA, Tappe S, Stern RA, Webb SJ, Ashwal LD (2016) Early Archaean tectonics and
606 mantle redox recorded in Witwatersrand diamonds. Nature Geosci:
607 DOI:10.1038/NGEO2628
608 Smith CB (1983) Pb, Sr and Nd isotopic evidence for sources of southern African Cretaceous
609 kimberlites. Nature 304: 51-54
610 Smith CB, Allsopp HL, Kramers JD, Hutchinson G, Roddick JC (1985) Emplacement ages of
611 Jurassic–Cretaceous South African kimberlites by the Rb–Sr method on phlogopite
612 and whole rock samples. Trans Geol Soc S Afr 88(2): 249–266.
613 South African Committee for Stratigraphy (SACS), Kent LE (Comp) (1980) Stratigraphy of
614 South Africa Part 1: Lithostratigraphy of the Republica of South Africa, South West

615 Africa/Namibia, and the Republics of Bophuthatswana, Transkei and Venda. Handbk
616 Geol Soc S Afr 8, 690pp
617 Steiger RH, Jäger E (1977) Subcommission on geochronology: Convention on the use of
618 decay constants in geo- and cosmochronology. Earth Planet Sci 36:359–362
619 Stollhofen H, Werner M, Stanistreet IG, Armstrong RA (2008) Single-zircon U-Pb dating of
620 Carboniferous-Permian tuffs, Namibia and the intercontinental deglaciation cycle
621 framework. Geol Soc Amer Spec Paper 441: 83-96
622 Sutherland DG (1982) The transport and sorting of diamonds by fluvial and marine processes.
623 Econ Geol 77:1613–1620
624 Thomas RJ, Agenbacht ALD, Cornell DH, Moore JM (1994) The Kibaran of southern Africa:
625 tectonic evolution and metallogeny. Ore Geol Rev 9:131–160
626 Turner G, Cadogan PH (1974) Possible effects of 39Ar recoil in ^{40}Ar-^{39}Ar dating. Geochim
627 Cosmochin Acta Suppl 5 (Proc Fifth Lunar Sci Conf): 1601-1615
628 Van Wyk JP, Pienaar LF (1986) Diamondiferous gravels of the lower Orange River,
629 Namaqualand. In: Anhausser CR, Maske S (eds) Mineral Deposits of Southern Africa,
630 II. Geol Soc S Afr, pp 2309–2321
631 Visser JNJ (1997) Deglaciation sequences in the Permo-Carboniferous Karoo and Kalahari
632 basins of southern Africa: a tool in the analysis of cyclic glaciomarine basin fill.
633 Sedimentol 44:507–521

Figure captions:

Fig. 1 Locality map of southern Africa showing the outline of the Archean Kaapvaal Craton, the Dwyka Group outcrop (blue), younger Karoo Basin lithologies (green), the Namibian and Namaqualand diamond placer deposits, and the distribution of kimberlites and related rocks (modified from Ayers et al., 1998; Jelsma et al., 2004; and Jacobs et al., 2008). Some individual kimberlite and orangeite localities are shown in figure 5,

Fig. 2 Schematic diagram illustrating argon diffusion from clinopyroxene (cpx) inclusions in diamond. Under high temperature conditions (in the mantle or kimberlite melt), most radiogenic ^{40}Ar ($^{40}Ar^*$), produced by decay of ^{40}K in clinopyroxene, diffuses to the diamond/inclusion interface zone. Low, post-eruption temperatures permit retention of $^{40}Ar^*$ in clinopyroxene. Therefore, $^{40}Ar/^{39}Ar$ analyses of extracted inclusions give ages approaching the time of kimberlite (or related rock) emplacement. Acquisition of genesis ages requires laser drilling and fusion of the clinopyroxene inclusion, to sample both inclusion and interface argon reservoirs (e.g., Burgess et al., 2004).

Fig. 3 Photo showing peridotitic clinopyroxene inclusion fragments extracted from diamond NQ109, Namaqualand detrital diamond deposits. Note the emerald green colour characteristic of Cr-diopside, and the small black graphite crystals on inclusion surfaces, indicating a decrease in internal pressure (see Phillips et al., 2004a for discussion).

Fig. 4a $^{40}Ar/^{39}Ar$ high temperature apparent ages for clinopyroxene inclusions extracted from Namaqualand detrital diamonds and analysed using an MM5400 mass spectrometer.

660 The data are plotted in age order. Also shown are the age ranges for Late Cretaceous
661 (Group I) kimberlites and orangeites (aka Group II kimberlites), as well as U-Pb
662 zircon constraints on the timing of Dwyka tillite deposition (e.g. Stollhofen et al.,
663 2008). Error bars indicate 2σ-uncertainties in age determinations.
664
665 **Fig. 4b** $^{40}Ar/^{39}Ar$ high temperature apparent ages for clinopyroxene inclusions extracted from
666 Namaqualand detrital diamonds and analysed using a multi-collector ARGUSVI mass
667 spectrometer. The data are plotted in age order. As above, age ranges are shown for
668 Late Cretaceous Group I kimberlites and orangeites, and the timing of Dwyka tillite
669 deposition (Stollhofen et al., 2008). Error bars indicate 2σ-uncertainties in ages.
670
671 **Fig. 5a** Reconstructed paleo-drainage patterns for southern Africa in the Cretaceoous period,
672 prior to ~90 Ma, infer the existence of a northerly 'Kalahari' River and a southerly
673 'Karoo' River, both flowing westward from the hinterland (modified from de Wit et
674 al, 1999). Kimberlite locality information is as follows (filled blue symbols indicate
675 major kimberlite mines; open symbols are orangeites): F=Finsch (ca.118 Ma); L=Lace
676 (ca.132 Ma); D = Dokolwayo (ca.200 Ma); J=Jwaneng (ca.240 Ma); P=Premier
677 (~1200 Ma). Kimberlite ages are from Jelsma et al. (2004) and references therein.
678
679 **Fig. 5b** Palaeo-drainage reconstruction for the Late Cretaceous to early Paleogene period,
680 when the Orange River is purported to have captured the 'Karoo' River (modified
681 from de Wit, 1999). Kimberlite locality information as per Fig.5a. Additional post-90
682 Ma kimberlites include: K=Kimberley (ca.85 Ma); Kof=Koffiefontein (ca.90 Ma);
683 Mo=Monastery (ca.86 Ma). Kimberlite ages are from Jelsma et al. (2004) and
684 references therein.
685

Table 1 Available age data for known diamondiferous kimberlites and orangeites in southern Africa

Rock type	Age (Ma)	Location	Locality examples	References
Kimberlite	80 - 90	Southern Africa	Kimberley, Orapa	Allsopp and Barrett (1975); Davis (1977)
Orangeite	118 - 122	Barkley West, South Africa	Newlands, Finsch, Pniel	Smith et al. (1985); Phillips et al. (1991)
Orangeite	128 - 132	Kroonstad, South Africa	Voorspoed, Lace, Besterskraa	Phillips et al. (1998, 1999)
Orangeite	140 - 145	Swartruggens, South Africa	Swartruggens dykes	Allsopp and Barrett (1975); Phillips (1991)
Orangeite	~200	Swaziland	Dokolwayo pipe	Allsopp and Roddick (1984)
Kimberlite	~240	Southern Botswana	Jwaneng DK2 pipe	Kinny et al. (1989)
Kimberlite	500 - 530	South Africa, Zimbabwe	Marnitz, Venetia, Colossus	Allsopp et al. (1985); Phillips et al. (1999)
Kimberlite	~1200	Cullinan, South Africa	Premier pipe	Kramers and Smith (1983)
Kimberlite	~1350	Southeast Botswana	Martins Drift cluster	Pers. Comm. In Jelsma et al. (2004)

Table 2 Sample attributes of Batch A clinopyroxene inclusions extracted from Namaqualand detrital diamonds.

Sample No	Paragenesis	Mineral	No Inclusion fragments	Size of inclusions (microns)	Estimated weight[a] (μg)	Estimated weight[b] (μg)	Estimated K (ppm)[c]	Total-gas age (Ma) (±2σ)	High Temp age (Ma) (±2σ)
NQ1	Peridotitic	cpx	3	200x200x150; 300x200x100; 300x200x100	59	27	14436	155.2 ± 3.4	150.8 ± 2.4
NQ2	Peridotitic	cpx	1	200x200x100	13	11	420	169 ± 162	154 ± 90
NQ3	Eclogitic	cpx	2	120x100x100; 100x80x80	6	5	3182	469 ± 74	183 ± 19
NQ4	Peridotitic	enstatite	3	100x100x60; 150x100x60; 100x100x20	6	nd[d]	nd[d]	344 ± 266	nd[d]
NQ5	Eclogitic	cpx	3	200x200x100; 200x100x100; 200x100x100	26	5	1509	166 ± 92	167 ± 38
NQ6	Eclogitic	cpx	3	500x200x30; 200x200x30; 150x50x30	15	31	3516	184.9 ± 9.0	175.2 ± 5.6
NQ7	Peridotitic	cpx	1	120x100x100; 100x80x80	6	3	2290	nd	102 ± 68
NQ8	Eclogitic	cpx	2	300x200x100; 300x200x50	30	28	3470	279 ± 12	261.1 ± 7.0
NQ9	Eclogitic (?)	cpx (?)	2	700x200x100; 400x300x200	79	4	1837	nd	nd
NQ10	Eclogitic (?)	cpx (?)	2	500x400x300; 200x120x120	208	82	438	283 ± 30	150 ± 16
NQ11	Peridotitic	cpx	1	500x200x200	66	1	386	nd	nd
NQ12	Eclogitic	cpx	3	200x160x100; 160x100x80; 200x150x100	25	22	3955	299.8 ± 9.0	252.2 ± 5.2
NQ13	Eclogitic	cpx	2	700x500x300; 500x400x150	446	203	1781	168.4 ± 3.4	131.4 ± 2.2
NQ14	Eclogitic	cpx	6	300x200x80; 300x100x50; 200x200x60; 200x150x50; 120x120x80; 100x100x50	28	24	3749	189 ± 10	188.6 ± 6.2
NQ15	Eclogitic (?)	cpx (?)	2	400x300x150; 400x300x100	99	3	500	nd	nd
NQ16	Eclogitic	cpx	2	250x200x200; 150x120x100	39	30	803	1351 ± 58	1341 ± 38
NQ17	Peridotitic	cpx	1	200x100x100	7	8	1995	200 ± 52	192 ± 30
NQ18	Eclogitic	cpx	6	200x120x100; 200x100x50; 120x100x150; 120x80x80; 80x80x60; 80x80x60;	22	16	1868	188 ± 26	194 ± 15
NQ19	Eclogitic	cpx	1	200x120x100	8	6	3354	160 ± 40	117 ± 44
NQ20	Eclogitic	cpx	8	250x200x150; 250x100x100; 150x100x80 100x100x80; 100x100x80; 100x80x80; 100x80x50; 80x80x50	47	33	2510	201 ± 13	150.0 ± 7.0
NQ21	Peridotitic	cpx	3	200x100x120; 120x100x50; 120x120x100	15	21	2735	122 ± 14	124.9 ± 8.0
NQ22	Peridotitic	cpx	2	100x80x50; 100x50x50	2	1	2730	nd	nd
NQ23	Eclogitic	cpx	4	250x200x60; 150x150x50; 200x100x80; 200x100x80	24	16	684	323 ± 88	193 ± 51
NQ24	Peridotitic	cpx	3	300x250x80; 300x200x120; 200x100x100	50	1	1565	361 ± 320	nd
NQ25	Eclogitic	cpx	6	350x200x100; 300x200x150; 200x100x100; 250x200x150; 150x100x100; 200x120x80	95	100	4403	911.9 ± 8.8	811.4 ± 6.4
NQ26	Eclogitic	cpx	6	650x500x250; 450x275x200; 350x300x200; 300x200x200; 300x200x200; 200x120x120	508	396	3071	255.1 ± 2.6	245.9 ± 2.0
NQ27	Eclogitic (?)	cpx (?)	2	300x200x100; 300x200x200	59	<1	6587	nd	2268 ± 562
NQ28	Eclogitic		2	500x300x200; 300x120x100	111	111	2731	267.3 ± 5.6	260.0 ± 4.4
NQ29	Eclogitic		2	400x300x200; 300x200x100	99	52	5045	171.2 ± 7.6	120.1 ± 6.2
NQ30	Eclogitic		9	350x200x100; 300x100x100; 400x300x100; 400x300x100; 150x100x100; 400x200x60; 250x150x100; 150x120x100; 200x100x60; 200x100x80	161	156	1869	191.9 ± 3.6	193.5 ± 4.4
NQ31	Peridotitic		2	300x200x100; 200x200x150	20	36	279	152 ± 106	nd
NQ32	Eclogitic		6	400x300x200; 500x400x350; 200x200x50; 150x100x50; 150x100x100; 200x200x50	331	127	46	3921 ± 180	3679 ± 195
NQ33	Eclogitic		3	600x400x400; 400x300x150; 200x200x150	396	222	1551	247.3 ± 5.6	231.2 ± 4.6
NQ34	Peridotitic		1	500x300x200	99	47	1011	142 ± 27	118 ± 26
NQ35	Eclogitic		3	200x200x70; 100x100x70; 200x100x100	18	15	501	824 ± 234	455 ± 276
NQ36	Eclogitic		1	100x100x80	3	3	4863	136 ± 37	136 ± 37
NQ37	Eclogitic		1	450x400x200	119	148	4216	262 ± 13	262 ± 12
NQ38	Eclogitic		2	300x200x200; 300x200x200	79	32	nd	nd	nd
NQ39	Peridotitic		3	100x100x100; 100x50x50; 150x100x100	9	3	5666	103 ± 42	117 ± 39
NQ40	Eclogitic		3	200x100x100; 200x100x30; 150x100x30	10	9	972	174 ± 83	236 ± 69
NQ41	Eclogitic		1	400x200x200	53	39	512	1634 ± 75	920 ± 119
NQ42	Peridotitic		2	400x300x100; 300x300x100	69	49	2956	252 ± 14	238 ± 12
NQ43	Eclogitic		9	300x200x150; 250x200x100; 250x120x100; 100x100x50; 100x100x30; 100x50x50; 100x50x50; 100x80x50; 100x50x50	63	32	950	170 ± 50	162 ± 36
NQ44	Peridotitic		6	200x200x50; 200x200x100; 180x120x100; 150x100x50; 100x50x50; 100x50x50	31	18	3012	242 ± 129	140 ± 60
NQ45	Peridotitic	enstatite	1	250x150x100	12	nd	nd	nd	nd
NQ46	Eclogitic	cpx (?)	2	200x200x60; 200x100x60	12	nd	nd	nd	nd
NQ47	Peridotitic	enstatite	1	200x100x50	3	<1	nd	nd	nd
NQ48	Peridotitic	cpx	9	500x300x200; 400x200x100; 300x200x50; 200x100x50; 200x200x100; 200x200x100; 200x100x60; 100x100x80; 200x150x50	177	117	221	nd	nd

[a] Inclusion weights estimated from size measurements, assuming a density of 3.3 g.cm^{-3}.

[b] Weight (μg) = (4.01 x 10^9) x (moles$^{37}Ar_{CaK}$/Ca) x (λ/λ_e) x ($K/^{40}K$) x (α/J), where α = 1.8 ± 0.1; $(Ca)^{ECpx}$ = 10 wt.%; $(Ca)_{PCpx}$ = 14 wt.%.

[c] K (ppm) = 9756 x $(Ca)_{Cpx}$ x $(K/Ca)_{unk}$; (Ca)ECpx = 10 wt.%; (Ca)PCpx = 14 wt.%.

[d] nd = not determined.

Table 3 Sample attributes of Bacth B clinopyroxene inclusions extracted from Namaqualand detrital diamonds.

Sample No	Paragenesis	Mineral	No Inclusion fragments	Size of inclusions (microns)	Estimated weight[a] (μg)	Estimated weight[b] (μg)	Estimated K (ppm)[c]	Total-gas age (Ma) (±2σ)	High Temp age (Ma) (±2σ)
NQ100	Eclogitic	cpx cpx	7	300x300x150, 200x100x100, 200x150x100 100x100x60, 150x100x80, 150x100x80	71	40	4443	312.8 ± 8.8	290.4 ± 2.0
NQ101a	Eclogitic	cpx	1	300x200x150	30	45	1464	272.9 ± 4.8	227.9 ± 2.0
NQ101b			1	300x250x200	49	12		153.1 ± 6.0	137.2 ± 5.2
NQ102	Peridotitic	cpx	1	200x150x100	10	5	3701	289.5 ± 5.8	254.3 ± 3.2
NQ103	Peridotitic	cpx	1	400x200x100	26	13	287	193 ± 16	193 ± 16
NQ104	Eclogitic	cpx	1	100x100x100	3	1	5687	343.0 ± 4.8	343.0 ± 4.8
NQ105	Peridotitic	cpx	1	500x300x150	74	41	200	140 ± 13	140 ± 13
NQ106	Not recovered	cpx	7	250x200x150, 200x150x100, 150x100x100 100x80x80, 200x100x100, 200x100x50 200x100x100	58	nd[d]	nd[d]	nd[d]	nd[d]
NQ107	Eclogitic	cpx	1	200x200x200	26	12	1831	324.9 ± 2.0	324.9 ± 2.0
NQ108	Eclogitic	cpx	3	200x250x60, 300x200x100, 200x100x100	36	25	3874	239.6 ± 0.4	239.6 ± 0.4
NQ109	Peridotitic	cpx	12	450x300x140, 400x150x100:,150x100x100 350x150x100, 300x150x100, 100x100x100 120x100x100, 200x100x100, 200x100x50 100x50x50, 100x50x50,100x50x50	143	86	291	208.3 ± 7.0	227.2 ± 5.2
NQ110	Peridotitic	cpx	3	300x200x150, 200x200x100, 200x100x100	56	29	5483	303.2 ± 0.6	303.2 ± 0.6
NQ111	Eclogitic	cpx	3	500x100x50, 350x100x60, 200x200x200	42	51	4285	210.8 ± 0.8	210.8 ± 0.8
NQ112	Eclogitic	cpx	5	350x250x120, 300x200x150, 100x100x80 200x100x80, 200x100x50	76	36	5405	564.1 ± 1.0	564.1 ± 1.0
NQ113	Peridotitic	cpx	1	600x300x300	178	44	2601	236.8 ± 1.2	235.5 ± 0.6
NQ114	Peridotitic	cpx	1	200x200x200	26	12	5083	239.5 ± 1.0	239.5 ± 1.0
NQ115	Eclogitic	cpx	1	250x200x100	17	12	3183	194.8 ± 2.4	194.8 ± 2.4
NQ116	Peridotitic	enstatite	1	100x100x100	3	nd	nd	nd	nd
NQ117	Eclogitic	cpx	1	250x150x100	12	10	2517	141.0 ± 3.6	141.0 ± 3.6
NQ118	Eclogitic	cpx	2	200x100x100, 200x150x100	17	7	5870	186.9 ± 1.8	186.9 ± 1.8
NQ119	Eclogitic	cpx	3	250x200x100, 200x100x80, 200x100x50	25	23	2451	127.0 ± 2.0	123.4 ± 1.6
NQ120	Peridotitic	cpx	1	700x500x100	11	1	856	nd	nd
NQ121	Eclogitic	cpx	2	500x300x120, 200x150x100	69	41	3338	294.6 ± 4.2	254.4 ± 1.0
NQ122	Peridotitic	cpx	2	350x150x100, 100x100x80	20	8	6302	152.1 ± 2.4	128.4 ± 1.8
NQ123	Peridotitic	cpx	1	500x500x300	248	73	276	293 ± 13	283.0 ± 5.4
NQ124	Eclogitic	cpx	2	350x200x200, 200x150x100	56	29	717	1399 ± 21	668.7 ± 5.0
NQ125	Peridotitic	cpx	1	400x300x150	59	26	1862	29.0 ± 4.0	121.5 ± 3.4
NQ126	Eclogitic	cpx	3	600x100x100, 100x100x60x 100x100x120	26	12	3675	247.9 ± 1.6	245.1 ± 1.0
NQ127	Eclogitic	cpx	5	400x200x200, 300x200x200, 250x100x100 150x150x50, 100x100x100	108	54	1755	264.3 ± 1.2	252.8 ± 0.6
NQ128	Not recovered	cpx	4	300x200x150, 300x100x100, 200x150x100 150x100x50	52	nd	nd	nd	nd
NQ129	Eclogitic	cpx	4	200x200x100, 200x100x50, 200x100x50 100x100x50	20	8	2110	186.8 ± 4.0	181.2 ± 3.8
NQ130	Eclogitic	cpx	1	250x200x100	17	5	880	370 ± 38	287 ± 15
NQ131	Eclogitic	cpx	1	200x200x200	26	20	2124	379.4 ± 4.6	365.2 ± 1.4
NQ132	Eclogitic	cpx	1	350x150x100	17	6	1178	238 ± 15	240.3 ± 8.6
NQ133	Peridotitic	cpx	1	400x200x100	26	4	155	191 ± 108	191 ± 108
NQ134	Eclogitic	cpx	1	200x100x100	7	7	1163	178 ± 15	126.0 ± 8.4
NQ135	Eclogitic	cpx	3	100x100x80, 120x100x50, 200x150x100	15	7	5666	191.4 ± 2.2	185.7 ± 1.4

[a] Inclusion weights estimated from size measurements, assuming a density of 3.3 $g.cm^{-3}$.

[b] Weight (μg) = $(4.01 \times 10^{9}) \times (moles\ ^{37}Ar_{CaK}/Ca) \times (\lambda/\lambda_e) \times (K/^{40}K) \times (\alpha/J)$, where $\alpha = 1.8 \pm 0.1$; $(Ca)^{ECpx} = 10$ wt.%; $(Ca)_{PCpx} = 14$ wt.%.

[c] K (ppm) = $9756 \times (Ca)_{Cpx} \times (K/Ca)_{unk}$; $(Ca)_{Cpx} = 10$ wt.%, the average for eclogitic cpx inclusions in Orapa diamonds.

[d] nd = not determined.

Colour Figure 1

Click here to download Colour Figure Fig1_localitymap.eps

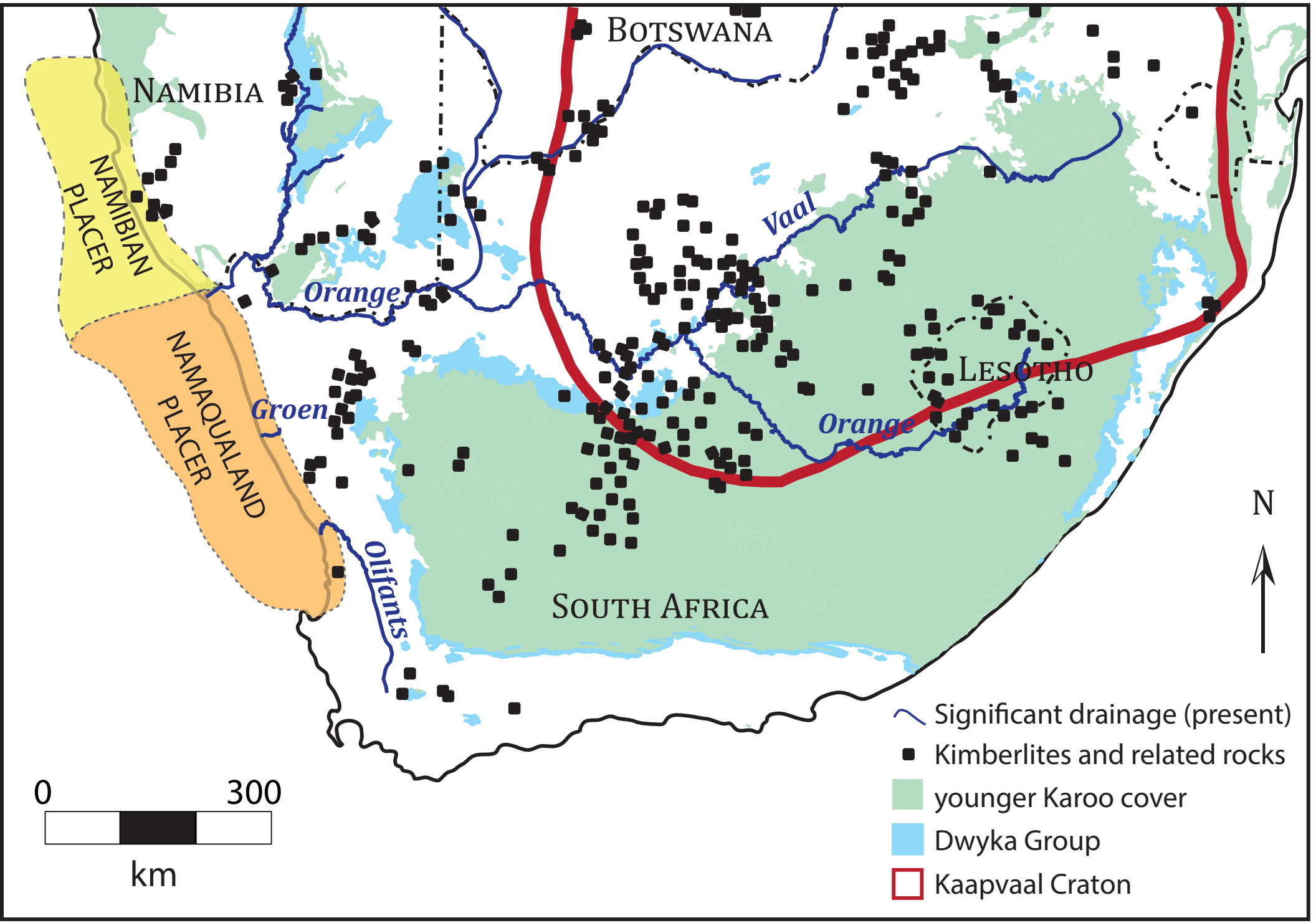

Fig. 2

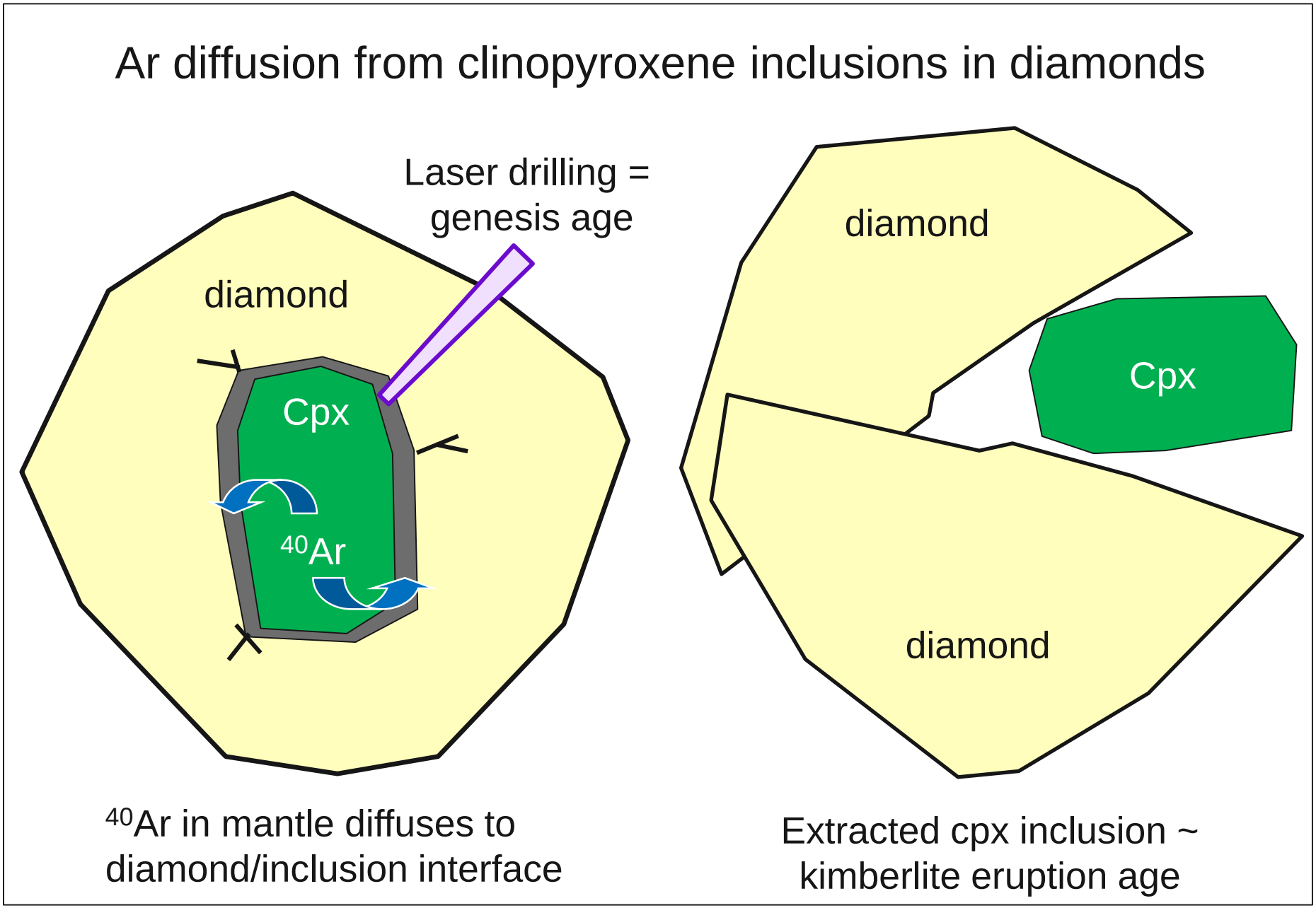

Fig. 3

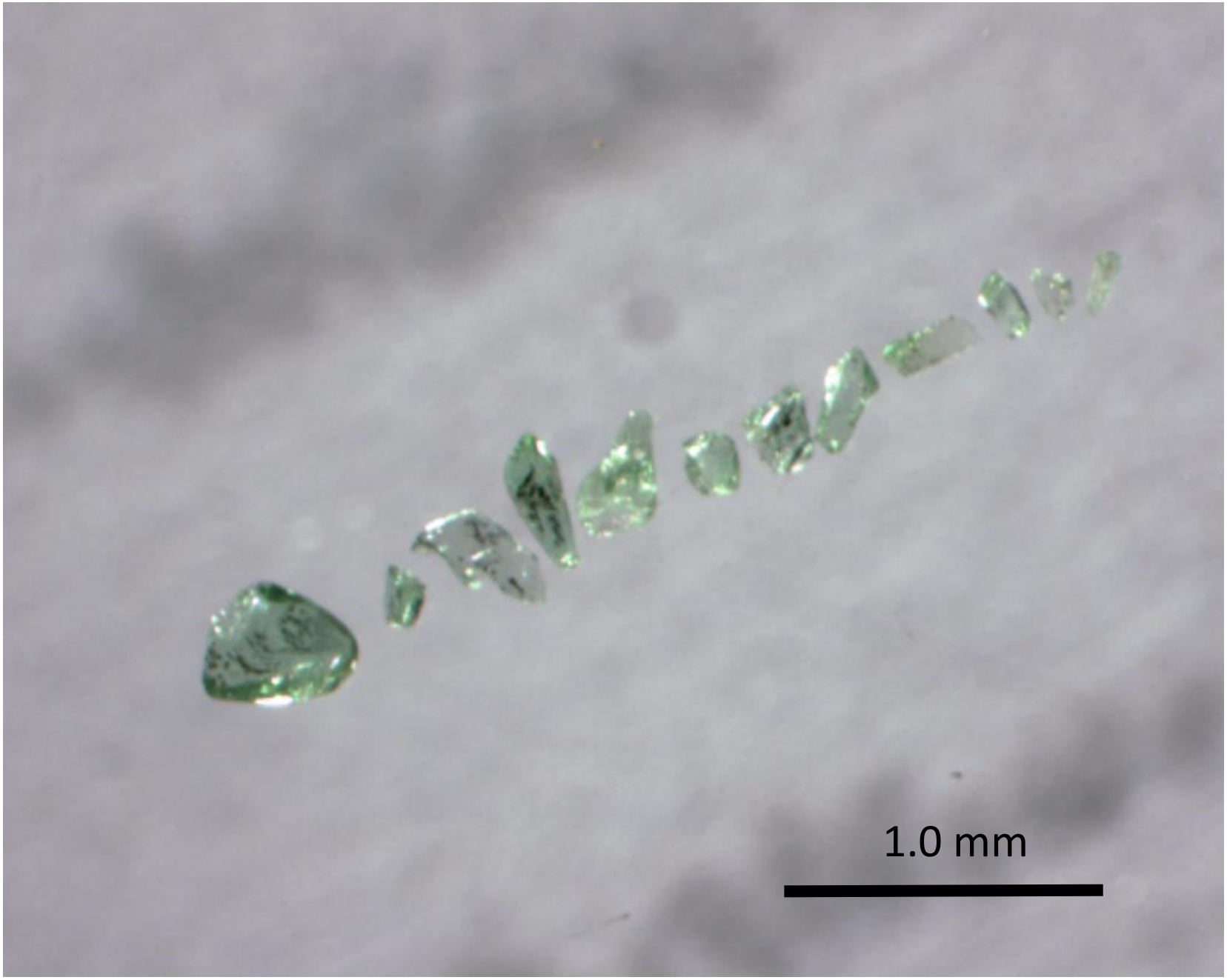

Fig. 4a

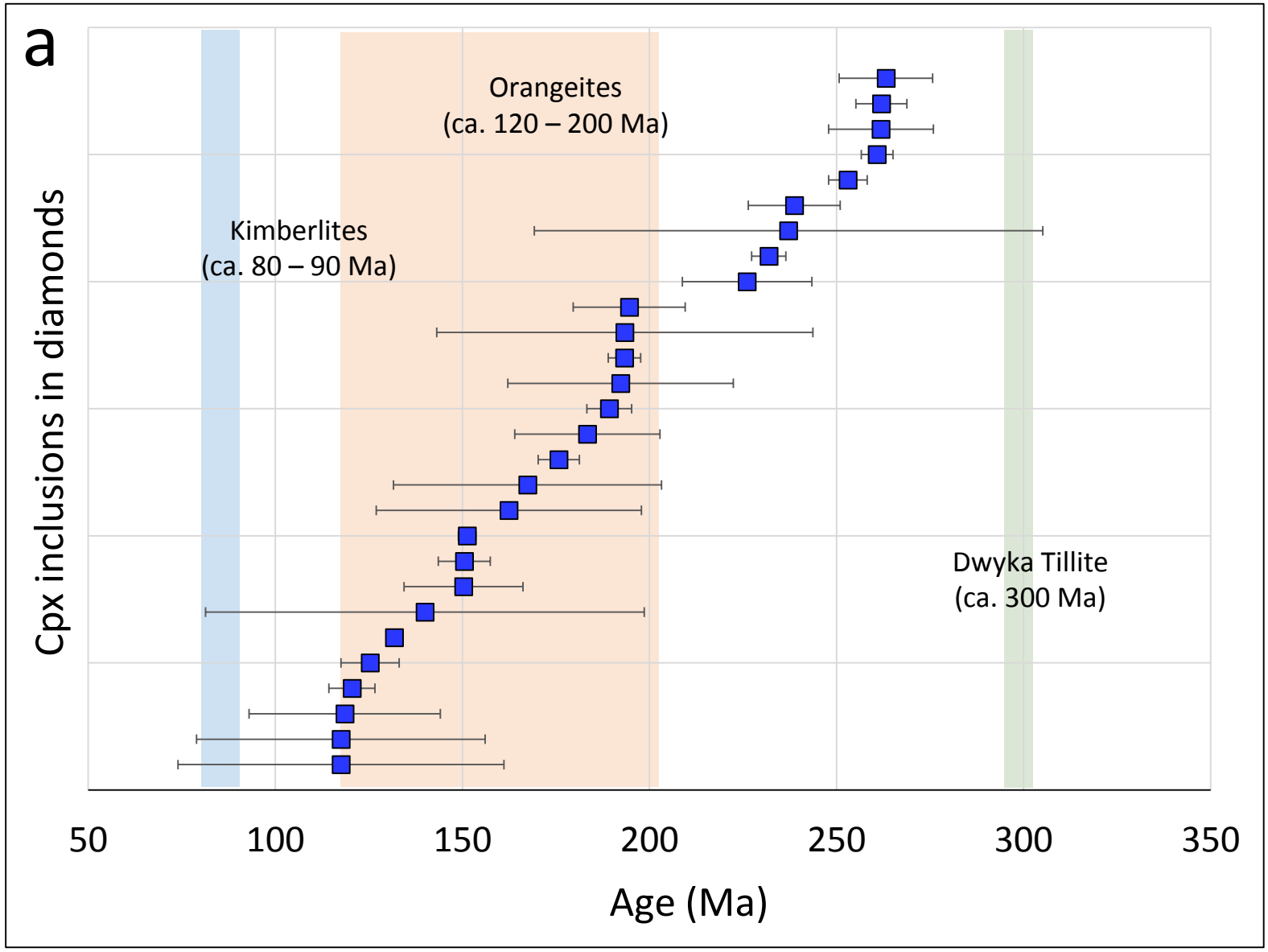

Colour Figure 4b

Click here to download Colour Figure Figure4b_Revised.pptx

Fig. 4b

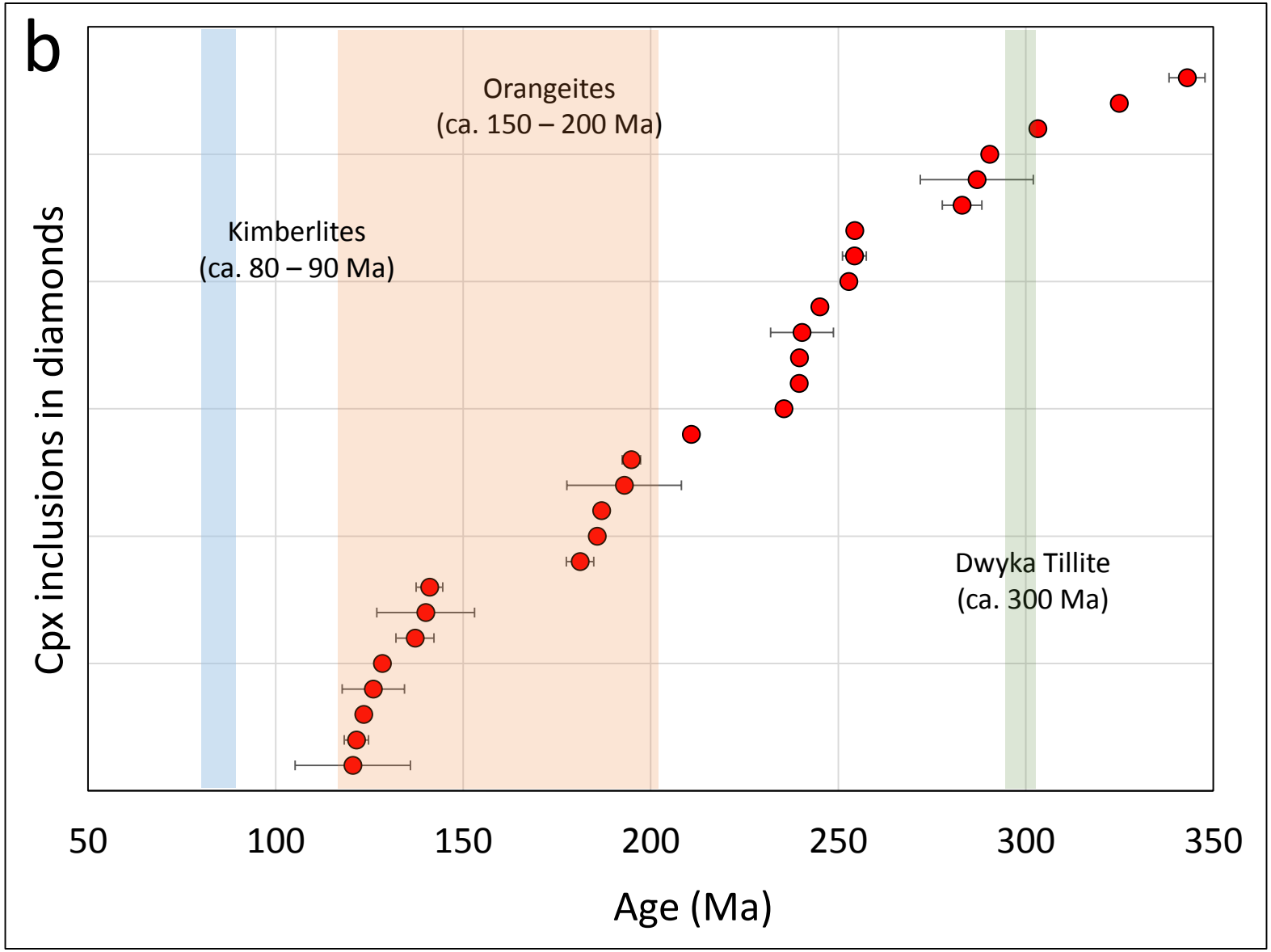

Colour Figure 5a

Click here to download Colour Figure Fig5a_Pre90Ma.eps

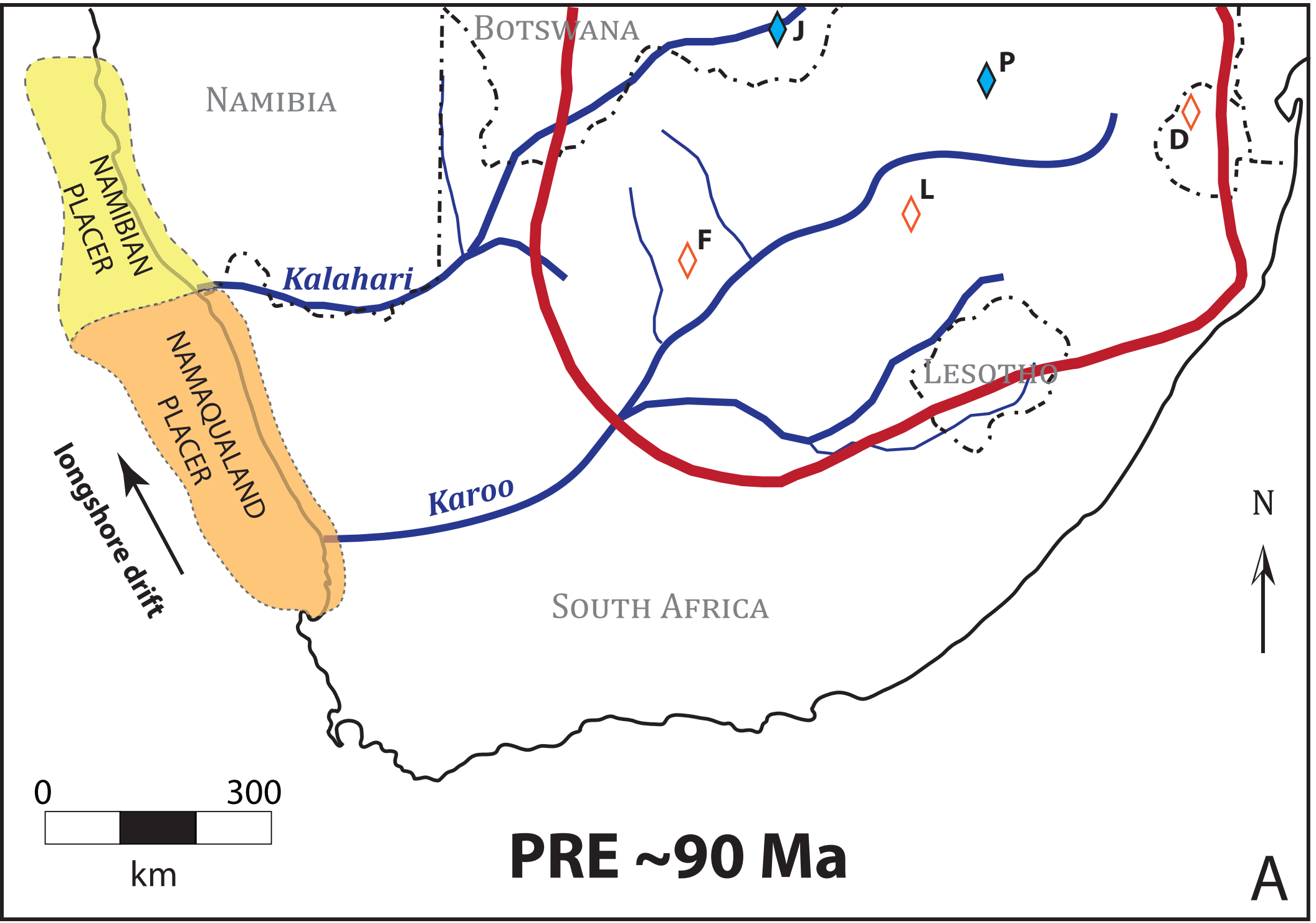

Colour Figure 5b

Click here to download Colour Figure Fig5b_post90Ma.eps

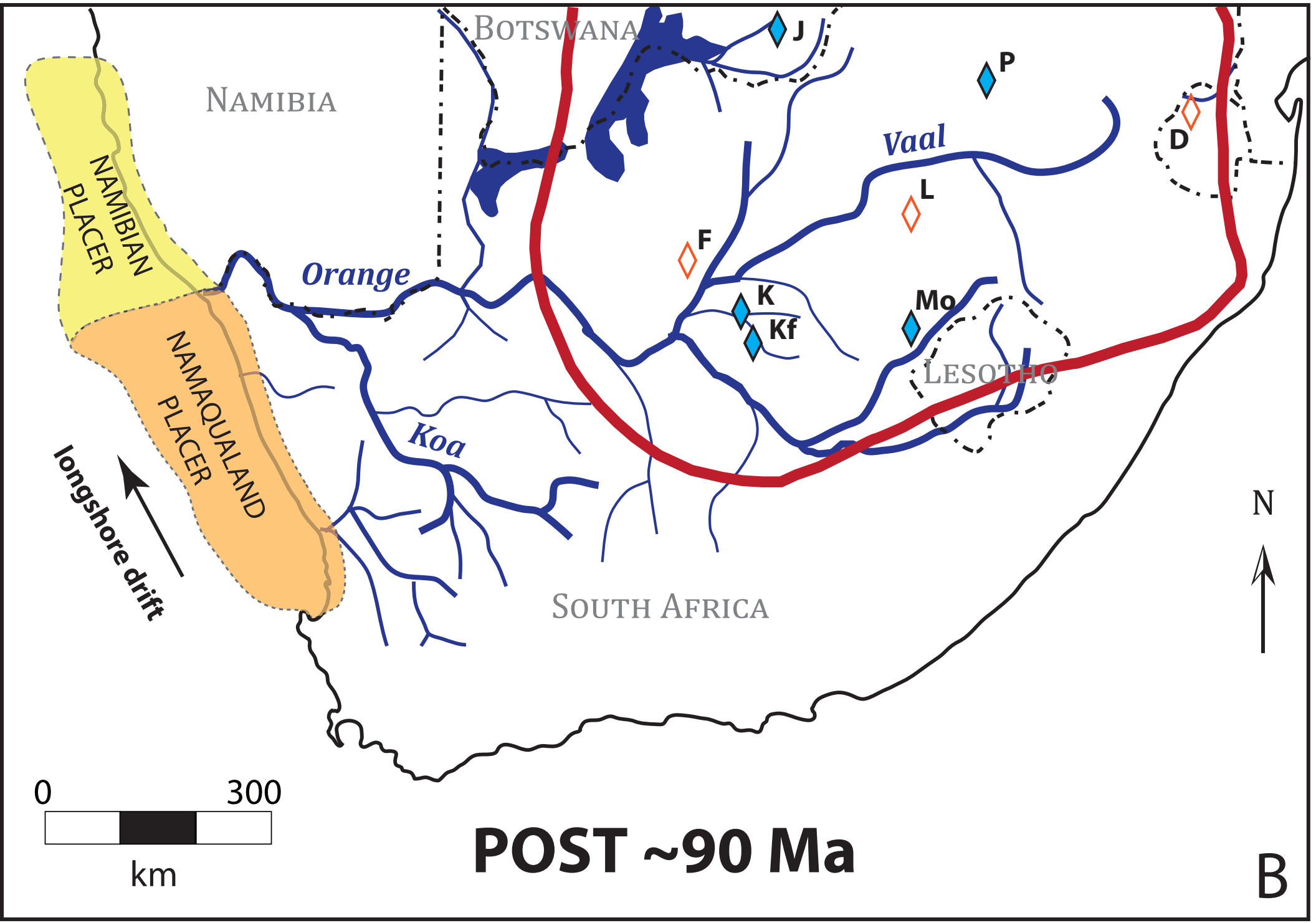

Supplementary TableA1

Click here to download Table
Supp_TableA1_ArData_BatchA_Namaqua_Cpx_Revised.xlsm

Table A1 MM5400 $^{40}Ar/^{39}Ar$ analytical results for Batch A clinopyroxene inclusions from Namaqualand detrital diamonds

Sample ID	Step No	Cum.% ^{39}Ar	^{40}Ar (x10^{-15} moles)	±1σ	^{39}Ar (x10^{-15} moles)	±1σ	^{38}Ar (x10^{-16} moles)	±1σ	^{37}Ar (x10^{-16} moles)	±1σ	^{36}Ar (x10^{-16} moles)	±1σ	Ca/K	±1σ	^{a}%^{40}Ar*	$^{40}Ar^*/^{39}Ar$	±1σ	Age (Ma)	±1σ^{b}
Experiments with negligible ^{40}Ar* or ^{39}Ar in red text.																			
UM#2: J-Value^{c} = 0.004993 ± 0.000016																			
NQ1	1	0.8	0.9728	0.0051	0.0049	0.0003	0.0031	0.0007	0.0086	0.0016	0.0192	0.0011	3.1	0.6	41.7	83.10	8.45	626.1	53.8
	2	100.0	11.0093	0.0535	0.5955	0.0022	0.0058	0.0024	3.2371	0.0357	0.0196	0.0019	9.5	0.1	94.7	17.52	0.14	151.3	1.2
	Total^{d}															18.05	0.21	155.7	1.8
NQ2	1	32.0	0.5072	0.0038	0.0022	0.0001	0.0060	0.0006	0.0026	0.0019	0.0154	0.0014	2.0	1.5	10.3	23.65	19.38	201.3	156.1
	2	100.0	0.5435	0.0043	0.0047	0.0002	0.0029	0.0006	1.2769	0.0124	0.0156	0.0008	477.3	23.2	15.4	17.92	5.47	154.6	45.2
	Total															19.75	9.91	169.7	81.3
NQ3	1	9.4	1.4530	0.0086	0.0023	0.0002	0.0032	0.0008	0.0030	0.0025	0.0162	0.0015	2.3	2.0	67.0	429.35	45.83	2066	131
	2	100.0	0.8853	0.0116	0.0219	0.0002	0.0014	0.0005	0.4205	0.0040	0.0141	0.0008	33.6	0.4	53.0	21.43	1.22	183.4	9.9
	Total															59.67	5.40	470.4	37.5
NQ4	1	50.0	0.6773	0.0052	0.0022	0.0001	0.0036	0.0009	0.0043	0.0024	0.0179	0.0012	3.4	1.9	21.8	66.99	16.92	520.5	114.3
	2	100.0	0.7433	0.0053	0.0022	0.0001	0.0036	0.0006	0.0015	0.0011	0.0239	0.0014	1.2	0.9	5.2	nd^{e}	nd^{e}	nd^{e}	nd^{e}
	Total															42.23	18.04	345.2	134.2
NQ5	1	1.2	0.6430	0.0040	0.0002	0.0001	0.0019	0.0005	0.1350	0.0042	0.0218	0.0014	1570	1541	0.3	nd	nd	nd	nd
	2	5149.8	0.9022	0.0046	0.0124	0.0002	0.0013	0.0003	0.3301	0.0075	0.0223	0.0009	46.5	1.4	26.8	19.48	2.23	167.4	18.3
	Total															19.42	5.62	166.9	46.1
UM#2: J-Value = 0.004992 ± 0.000018																			
NQ6	1	0.7	0.9467	0.0044	0.0011	0.0001	0.0020	0.0009	0.0119	0.0029	0.0242	0.0007	18.2	5.0	24.3	202.41	31.97	1260	143
	2	100.0	4.1006	0.0216	0.1711	0.0011	0.0083	0.0011	2.7183	0.0313	0.0201	0.0017	27.8	0.4	85.5	20.50	0.34	175.7	2.8
	Total															21.70	0.55	185.5	4.5
NQ7	1	21.6	0.6305	0.0040	0.0022	0.0001	0.0010	0.0002	0.0259	0.1575	0.0215	0.0007	20.6	125.3	0.3	nd	nd	nd	nd
	2	100.0	0.7604	0.0049	0.0080	0.0002	0.0057	0.0006	0.3216	0.0049	0.0226	0.0011	70.4	2.0	12.3	11.70	4.02	102.4	34.2
	Total															9.39	5.35	82.6	46.0
NQ8	1	0.7	1.0224	0.0054	0.0011	0.0001	0.0044	0.0003	0.0038	0.0015	0.0213	0.0014	6.0	2.5	38.4	357.4	49.7	1847	161
	2	100.0	5.3660	0.0255	0.1507	0.0015	0.0035	0.0008	2.4351	0.0260	0.0219	0.0014	28.3	0.4	87.9	31.31	0.45	262.0	3.5
	Total															33.67	0.80	280.3	6.2
NQ9/1	1	37.4	0.7893	0.0048	0.0001	0.0001	0.0050	0.0007	0.0020	0.0024	0.0317	0.0013	40.7	63.5	0.3	nd	nd	nd	nd
	2	100.0	0.6430	0.0040	0.0001	0.0001	0.0019	0.0005	0.1433	0.0045	0.0218	0.0014	1730	1763	0.3	nd	nd	nd	nd
	Total															nd	nd	nd	nd
NQ9/2	1	50.0	0.7573	0.0054	0.0022	0.0001	0.0052	0.0008	0.0018	0.0030	0.0260	0.0010	1.4	2.4	0.3	nd	nd	nd	nd
	2	100.0	0.7159	0.0082	0.0022	0.0002	0.0019	0.0006	0.1317	0.0030	0.0248	0.0013	104.8	9.0	0.3	nd	nd	nd	nd
	Total															nd	nd	nd	nd
NQ10	1	15.0	1.7915	0.0122	0.0084	0.0004	0.0031	0.0005	0.0105	0.0027	0.0238	0.0013	2.2	0.6	60.7	129.38	7.43	898.9	40.7
	2	100.0	1.4344	0.0110	0.0477	0.0004	0.0036	0.0011	7.1237	0.0743	0.0205	0.0015	261.5	3.5	57.9	17.40	0.98	150.3	8.1
	Total															34.18	1.95	284.2	15.0
UM#2: J-Value = 0.004989 ± 0.000016																			
NQ11	1	61.7	0.7797	0.0051	0.0004	0.0001	0.0036	0.0003	0.0324	0.0013	0.0257	0.0013	135.6	40.2	2.7	nd	nd	nd	nd
	2	100.0	0.5739	0.0028	0.0003	0.0000	0.0019	0.0007	0.1047	0.0027	0.0187	0.0014	706.9	95.7	3.6	nd	nd	nd	nd
	Total															nd	nd	nd	nd
NQ12	1	7.1	1.8383	0.0108	0.0098	0.0001	0.0220	0.0011	0.1253	0.0019	0.0233	0.0012	22.4	0.4	62.5	117.56	3.88	832.6	22.0
	2	100.0	4.4889	0.0212	0.1285	0.0003	0.0045	0.0010	1.8246	0.0222	0.0206	0.0012	24.8	0.3	86.4	30.18	0.34	253.0	2.6
	Total															36.36	0.59	300.7	4.5
NQ13	1	12.6	4.4882	0.0243	0.0709	0.0006	0.0088	0.0013	1.6085	0.0212	0.0299	0.0012	39.7	0.6	80.3	50.88	0.76	408.1	5.5

	2	100.0	8.0962	0.0380	0.4926	0.0016	0.0047	0.0010	16.0291	0.1539	0.0207	0.0016	56.9	0.6	92.4	15.19	0.13	131.8	1.1
	Total															19.68	0.21	169.0	1.7
NQ14	1	1.2	0.6804	0.0048	0.0017	0.0001	0.0028	0.0004	0.0071	0.0034	0.0215	0.0013	7.2	3.5	6.6	26.04	23.08	220.3	183.9
	2	100.0	3.7331	0.0207	0.1378	0.0008	0.0003	0.0017	2.0680	0.0296	0.0229	0.0015	26.3	0.4	81.9	22.17	0.38	189.2	3.1
	Total															22.22	0.66	189.6	5.3
NQ15	1	23.2	0.7488	0.0049	0.0005	0.0000	0.0021	0.0007	0.0013	0.0006	0.0239	0.0012	4.7	2.1	5.9	90.83	75.64	674.2	468.7
	2	100.0	0.6379	0.0037	0.0016	0.0001	0.0033	0.0008	0.2317	0.0029	0.0215	0.0013	252.7	14.2	0.2	nd	nd	nd	nd
	Total															nd	nd	nd	nd
NQ16	1	0.4	0.7616	0.0058	0.0001	0.0001	0.0035	0.0003	0.0194	0.0007	0.0217	0.0019	241	137	15.8	854.8	628.6	2996	1076
	2	100.0	9.0176	0.0426	0.0378	0.0007	0.0029	0.0004	2.6122	0.0319	0.0219	0.0014	121.1	2.8	92.8	221.75	4.52	1343.9	19.3
	Total															224.10	6.84	1353.9	29.1
NQ17	1	8.8	0.6880	0.0065	0.0022	0.0001	0.0010	0.0004	0.0050	0.0024	0.0207	0.0012	4.0	1.9	11.2	34.97	16.69	290.1	127.9
	2	100.0	1.2298	0.0061	0.0229	0.0004	0.0030	0.0006	0.9752	0.0117	0.0242	0.0014	74.7	1.7	41.9	22.54	1.90	192.3	15.4
	Total															23.63	3.20	201.1	25.8
NQ18	1	3.6	0.6567	0.0055	0.0017	0.0001	0.0000	0.0008	0.0338	0.0034	0.0236	0.0011	35.0	3.8	0.3	nd	nd	nd	nd
	2	529.1	1.6235	0.0078	0.0456	0.0009	0.0024	0.0012	1.3774	0.0148	0.0197	0.0013	52.9	1.1	64.1	22.83	0.94	194.6	7.6
	Total															22.06	1.60	188.3	12.9
NQ19	1	50.4	1.0733	0.0105	0.0164	0.0004	0.0017	0.0005	0.2342	0.0044	0.0232	0.0012	25.0	0.8	36.1	23.63	2.32	201.0	18.7
	2	100.0	0.8418	0.0049	0.0161	0.0003	0.0015	0.0001	0.3059	0.0030	0.0211	0.0014	33.2	0.8	25.8	13.49	2.63	117.5	22.2
	Total															18.60	2.48	160.1	20.4
NQ20	1	10.1	1.6340	0.0084	0.0129	0.0004	0.0027	0.0007	0.2505	0.0034	0.0204	0.0017	34.0	1.0	63.0	79.79	4.56	604.5	29.4
	2	100.0	2.6743	0.0212	0.1147	0.0009	0.0040	0.0015	2.5837	0.0258	0.0228	0.0014	39.4	0.5	74.8	17.44	0.43	150.5	3.5
	Total															23.75	0.85	202.0	6.8
UM#2: J-Value = 0.004988 ± 0.000012																			
NQ21	1	2.5	0.6291	0.0050	0.0022	0.0001	0.0021	0.0009	0.0016	0.0012	0.0222	0.0011	1.3	1.0	0.3	nd	nd	nd	nd
	2	100.0	1.8063	0.0092	0.0854	0.0007	0.0042	0.0007	2.4996	0.0303	0.0194	0.0013	51.2	0.8	68.2	14.42	0.47	125.3	4.0
	Total															14.08	0.85	122.5	7.1
NQ22	1	6.8	0.5441	0.0039	0.0003	0.0001	0.0045	0.0004	0.0046	0.0019	0.0203	0.0016	23.1	10.8	0.4	nd	nd	nd	nd
	2	100.0	0.6268	0.0032	0.0048	0.0002	0.0031	0.0004	0.1424	0.0036	0.0199	0.0018	52.0	2.3	6.3	nd	nd	nd	nd
	Total															nd	nd	nd	nd
NQ23	1	13.8	1.0093	0.0062	0.0024	0.0002	0.0051	0.0008	0.1991	0.0048	0.0227	0.0013	148.1	16.1	33.6	144.03	22.75	976.7	119.2
	2	100.0	0.9742	0.0049	0.0147	0.0007	0.0045	0.0005	1.1894	0.0212	0.0217	0.0015	141.9	7.2	34.2	22.69	3.17	193.4	25.6
	Total															39.46	5.88	324.1	44.2
NQ24	1	71.2	0.7654	0.0037	0.0022	0.0001	0.0023	0.0007	0.0041	0.0012	0.0213	0.0010	3.3	1.0	17.7	61.64	13.46	483.6	92.7
	2	100.0	0.6359	0.0043	0.0009	0.0001	0.0023	0.0007	0.1499	0.0041	0.0230	0.0013	295.1	24.9	0.3	nd	nd	nd	nd
	Total															44.61	21.85	362.5	160.9
NQ25	1	12.7	23.0571	0.1182	0.0868	0.0007	0.0040	0.0014	1.0982	0.0114	0.0270	0.0013	22.1	0.3	96.5	256.48	2.44	1486.3	9.6
	2	100.0	68.8356	0.3269	0.5961	0.0006	0.0077	0.0014	7.5468	0.0710	0.0252	0.0016	22.2	0.2	98.9	114.23	0.57	813.5	3.3
	Total															132.31	0.81	914.3	4.4
UM#3: J-Value = 0.008731 ± 0.000019																			
NQ26/1	1	3.8	2.5951	0.0078	0.0653	0.0008	0.0147	0.0036	1.0825	0.0093	0.0111	0.0013	29.0	0.4	87.3	34.72	0.72	477.7	8.7
	2	100.0	28.0751	0.0741	1.6629	0.0021	0.0104	0.0058	29.9876	0.1425	0.0058	0.0031	31.6	0.2	99.2	16.78	0.07	246.7	1.0
	Total															17.46	0.10	255.9	1.3
NQ26/2	1	6.9	8.8143	0.0225	0.1096	0.0004	0.0375	0.0053	1.9502	0.0194	0.1669	0.0059	31.1	0.3	44.0	35.43	1.60	486.2	19.2
	2	30.8	31.7930	0.0734	0.3776	0.0022	0.1750	0.0025	6.8561	0.0482	0.8805	0.0076	31.8	0.3	18.2	15.29	0.64	226.1	8.8
	3	100.0	60.3779	0.1433	1.0924	0.0016	0.2747	0.0038	20.1451	0.1056	1.4416	0.0128	32.3	0.2	29.4	16.28	0.37	239.7	5.1
	Total															17.37	0.52	254.7	7.1
NQ27	1	49.1	26.5806	0.0680	0.0029	0.0002	0.1856	0.0038	0.0108	0.0018	0.8967	0.0088	6.5	1.1	0.3	nd	nd	nd	nd
	2	75.5	3.5872	0.0180	0.0016	0.0002	0.0257	0.0014	0.0248	0.0024	0.1062	0.0027	28.0	4.3	12.5	289.1	62.9	2272	281
	3	100.0	0.2054	0.0013	0.0014	0.0003	0.0004	0.0024	0.0142	0.0039	0.0087	0.0012	17.2	5.8	0.0	nd	nd	nd	nd
	Total															90.48	68.14	1050	600
NQ28	1	15.7	3.1789	0.0102	0.1301	0.0010	0.0344	0.0031	2.5660	0.0213	0.0141	0.0019	34.5	0.4	86.8	21.23	0.47	306.8	6.2
	2	100.0	12.8654	0.0380	0.6977	0.0046	0.0266	0.0070	14.3360	0.0712	0.0147	0.0021	36.0	0.3	96.5	17.81	0.16	260.8	2.2

	Total															18.35	0.21	268.1	2.8
NQ29	1	12.7	4.4052	0.0199	0.0905	0.0006	0.0099	0.0017	0.8903	0.0151	0.0400	0.0017	17.2	0.3	73.1	35.61	0.63	488.5	7.6
	2	100.0	14.8619	0.0534	0.6200	0.0026	0.0673	0.0029	6.9596	0.0341	0.3370	0.0040	19.6	0.1	33.0	7.91	0.21	120.5	3.1
	Total															11.44	0.27	171.7	3.8
NQ30	1	23.3	2.8902	0.0086	0.1843	0.0006	0.0171	0.0025	5.2742	0.0367	0.0185	0.0020	50.1	0.4	81.0	12.72	0.33	190.0	4.7
	2	100.0	8.2164	0.0376	0.6076	0.0020	0.0176	0.0034	18.3438	0.1077	0.0117	0.0028	52.8	0.4	95.6	12.95	0.16	193.3	2.2
	Total															12.90	0.20	192.6	2.8
UM#3: J-Value = 0.008771 ± 0.000019																			
NQ31	1	35.2	0.3089	0.0014	0.0097	0.0003	0.0059	0.0017	2.7696	0.0222	0.0058	0.0009	501.9	14.6	44.6	14.26	2.88	212.7	40.6
	2	100.0	0.3705	0.0012	0.0178	0.0003	0.0070	0.0002	4.9046	0.0300	0.0078	0.0024	482.5	7.5	37.4	7.80	4.07	119.3	60.2
	Total															10.07	3.65	152.7	53.1
NQ32	1	41.0	7.4641	0.0213	0.0065	0.0003	0.0166	0.0027	7.3730	0.0602	0.0167	0.0023	1986	100	93.4	1073.0	54.4	4227	83
	2	100.0	7.4133	0.0341	0.0094	0.0006	0.0036	0.0039	12.0088	0.0679	0.0086	0.0023	2245	138	96.6	764.8	47.5	3684	98
	Total															891.1	50.3	3927	90
NQ33	1	26.9	5.4565	0.0180	0.2531	0.0009	0.0186	0.0036	9.1222	0.0438	0.0135	0.0024	63.1	0.4	92.5	19.98	0.30	291.3	4.0
	2	100.0	11.2072	0.0473	0.6869	0.0042	0.0142	0.0030	24.6688	0.1877	0.0157	0.0028	62.8	0.6	95.7	15.64	0.17	231.9	2.3
	Total															16.81	0.20	248.1	2.8
NQ34	1	31.3	0.8225	0.0043	0.0409	0.0008	0.0032	0.0021	3.2160	0.0238	0.0101	0.0014	137.7	2.8	63.6	12.83	1.04	192.3	14.8
	2	100.0	1.2402	0.0064	0.0898	0.0007	0.0098	0.0035	6.8712	0.0442	0.0184	0.0027	133.8	1.3	56.0	7.74	0.88	118.6	13.0
	Total															9.33	0.93	141.9	13.6
NQ35	1	31.5	1.0439	0.0041	0.0063	0.0002	0.0030	0.0006	0.6145	0.0074	0.0053	0.0026	170.2	5.3	84.9	140.29	12.79	1447.2	90.8
	2	100.0	0.6573	0.0036	0.0137	0.0003	0.0025	0.0025	1.6180	0.0201	0.0070	0.0052	206.1	5.4	68.6	32.83	11.24	456.5	138.2
	Total															66.67	11.73	830.7	117.2
NQ36	1	100.0	0.4184	0.0028	0.0368	0.0006	0.0024	0.0031	0.4216	0.0064	0.0030	0.0016	20.1	0.4	78.3	8.93	1.28	136.0	18.8
UM#3: J-Value = 0.008811 ± 0.000019																			
NQ37	1	40.9	35.7654	0.0888	0.7019	0.0012	0.1561	0.0025	9.3276	0.0459	0.7892	0.0119	23.3	0.1	34.8	17.73	0.52	261.9	7.1
	2	100.0	55.7307	0.1422	1.0129	0.0040	0.2624	0.0034	13.3468	0.0635	1.2749	0.0150	23.1	0.1	32.4	17.83	0.46	263.2	6.4
	Total															17.79	0.49	262.7	6.7
NQ38	1	56.6	3.8659	0.0501	0.0836	0.0010	0.0185	0.0009	2.7677	0.0297	0.0812	0.0023	57.9	0.9	37.9	17.52	1.05	259.0	14.4
	2	100.0	106.3338	0.2611	0.0641	0.0010	0.7018	0.0070	2.1040	0.0157	3.6610	0.0315	57.4	1.0	0.0	nd	nd	nd	nd
	Total															9.92	7.13	151.1	104.2
NQ39	1	21.1	0.3078	0.0015	0.0100	0.0006	0.0072	0.0025	0.1358	0.0041	0.0094	0.0006	23.7	1.6	9.7	2.96	1.79	46.5	27.7
	2	100.0	0.3903	0.0022	0.0376	0.0004	0.0115	0.0016	0.5204	0.0076	0.0035	0.0017	24.2	0.4	73.4	7.64	1.32	117.5	19.7
	Total															6.66	1.42	102.8	21.3
NQ40	1	36.7	0.2779	0.0019	0.0090	0.0004	0.0014	0.0024	0.4861	0.0052	0.0082	0.0011	94.7	4.7	12.6	3.90	3.59	60.9	55.1
	2	100.0	0.3717	0.0015	0.0155	0.0003	0.0023	0.0022	0.9166	0.0125	0.0042	0.0013	103.6	2.5	66.3	15.95	2.49	237.2	34.7
	Total															11.52	2.89	174.4	41.7
NQ41	1	41.1	7.1617	0.0214	0.0223	0.0003	0.0064	0.0024	2.5042	0.0197	0.0162	0.0018	196.7	3.4	93.3	299.8	5.3	2332	23
	2	100.0	16.7850	0.0433	0.0319	0.0005	0.0906	0.0045	3.3978	0.0194	0.4861	0.0065	186.1	3.0	14.4	75.79	6.27	922.7	59.8
	Total															167.9	5.9	1638	38
NQ42	1	27.9	4.0956	0.0192	0.1111	0.0007	0.0230	0.0006	2.8624	0.0266	0.0645	0.0023	45.1	0.5	53.4	19.72	0.64	289.0	8.7
	2	100.0	10.1051	0.0293	0.2874	0.0008	0.0413	0.0029	7.6587	0.0469	0.1858	0.0042	46.6	0.3	45.6	16.06	0.45	238.7	6.3
	Total															17.08	0.50	252.9	7.0
UM#3: J-Value = 0.008850 ± 0.000020																			
NQ43	1	33.9	0.6045	0.0033	0.0282	0.0007	0.0342	0.0054	1.4339	0.0130	0.0090	0.0025	89.1	2.2	55.8	12.00	2.64	182.1	38.1
	2	100.0	0.7222	0.0033	0.0549	0.0009	0.0017	0.0027	3.4435	0.0280	0.0046	0.0023	109.7	2.0	80.8	10.64	1.24	162.4	18.1
	Total															11.11	1.71	169.1	24.7
NQ44	1	29.7	49.8586	0.1289	0.0441	0.0006	0.3246	0.0058	1.0315	0.0167	1.6382	0.0154	41.0	0.9	2.9	32.90	10.76	461.0	133.2
	2	100.0	26.6263	0.0812	0.1046	0.0005	0.1692	0.0013	2.8200	0.0158	0.8688	0.0066	47.2	0.3	3.6	9.11	2.02	140.0	29.9
	Total															16.17	4.62	241.3	64.1
NQ45	1	91.9	0.0989	0.0011	0.0006	0.0002	0.0025	0.0018	0.0460	0.0041	0.0059	0.0024	143.1	42.4	0.0	nd	nd	nd	nd
	2	100.0	0.1216	0.0018	0.0000	0.0002	0.0024	0.0027	0.0251	0.0036	0.0071	0.0017	890	3365	0.0	nd	nd	nd	nd

	Total															nd	nd	nd	nd
NQ46	1	100.0	19.5757	0.0477	0.0014	0.0001	0.1283	0.0023	0.0042	0.0037	0.6722	0.0082	5.3	4.7	0.0	nd	nd	nd	nd
NQ47	1	100.0	79.5331	0.2031	0.0036	0.0005	0.5250	0.0023	0.0283	0.0033	2.6940	0.0239	13.8	2.5	0.0	nd	nd	nd	nd
NQ48	1	13.8	1.5631	0.0046	0.0098	0.0003	0.0157	0.0025	3.1955	0.0187	0.0492	0.0018	569.6	18.1	6.9	11.04	5.38	168.2	78.2
	2	100.0	24.6926	0.0666	0.0612	0.0009	0.1590	0.0014	21.9033	0.1077	0.8178	0.0110	626.6	9.5	2.1	8.60	5.41	132.3	80.3
	Total															8.93	5.41	137.3	79.5

[a] $^{40}Ar^{*} = (^{40}Ar_{total} - {}^{40}Ar_{atmosphere})/^{40}Ar_{total}$

[b] Quoted errors are one sigma and exclude uncertainties in the J-value.

[c] J-values based on an age of 99.125 ± 0.076 Ma for GA1550 and MD-2 biotite (Phillips et al., 2017).

[d] Weighted average calculated using size of step weighting.

[e] nd = not determined (due to negligible $^{39}Ar_{K}$ and/or $^{40}Ar^{*}$

Supplementary TableA2

Click here to download Table
Supp_TableA2_ArData_Namaqualand_cpx_Revised.xlsm

Table A2 ARGUSVI $^{40}Ar/^{39}Ar$ laser step-heating analytical results[a] for Batch B clinopyroxene inclusions extracted from Namaqualand detrital diamonds

Sample ID	Step No	Laser Power	^{40}Ar (fA)[a,b]	±1σ	^{39}Ar (fA)[a,b]	±1σ	^{38}Ar (fA)[a,b]	±1σ	^{37}Ar (fA)[a,b]	±1σ	^{36}Ar (fA)[a,b]	±1σ	^{39}Ar (x10^{-14} mol)	Ca/K	±1σ	%^{40}Ar*	^{40}Ar*/^{39}Ar	±1σ	Cum.% ^{39}Ar	Apparent Age (Ma)	±1σ
Experiments with negligible ^{39}Ar in red text.																					
UM#68: J-Value[c] = 0.0262173912 ± 0.0000035131 (0.013%;1σ)																					
NQ100	1	0.2%	25.224	0.028	0.103	0.015	0.00090	0.00007	1.33	0.13	0.0048	0.0004	0.0004	22.61	4.02	94.3	231.09	34.52	0.2	3525.6	231.3
	2	1.5%	276.380	0.688	41.190	0.081	0.00128	0.00033	516.87	1.62	0.0068	0.0018	0.1462	21.96	0.08	99.3	6.661	0.025	100.0	290.4	1.0
	Total																7.220	0.111		312.8	4.4
NQ101a	1	0.3%	20.474	0.019	0.429	0.012	0.00085	0.00008	5.82	0.14	0.0045	0.0004	0.0015	23.73	0.88	93.4	44.56	1.26	2.8	1396.3	27.5
	2	1.5%	77.810	0.035	15.051	0.015	0.00032	0.00022	572.49	0.20	0.0017	0.0012	0.0534	66.56	0.07	99.3	5.136	0.024	100.0	227.9	1.0
	Total																6.229	0.058		272.9	2.4
NQ101b	1	0.4%	7.362	0.032	1.641	0.012	0.00059	0.00008	59.43	0.16	0.0031	0.0004	0.0058	63.39	0.51	87.4	3.921	0.083	40.3	176.5	3.6
	2	1.5%	7.618	0.024	2.426	0.010	0.00020	0.00009	92.49	0.17	0.0010	0.0005	0.0086	66.73	0.30	95.9	3.013	0.059	100.0	137.2	2.6
	Total																3.379	0.069		153.1	3.0
NQ102	1	0.4%	6.495	0.019	0.483	0.010	0.00021	0.00004	9.78	0.06	0.0011	0.0002	0.0017	35.47	0.77	95.0	12.78	0.29	12.4	521.4	10.4
	2	1.5%	19.832	0.031	3.422	0.007	0.00005	0.00008	72.15	0.06	0.0002	0.0004	0.0121	36.90	0.08	99.6	5.774	0.039	100.0	254.3	1.6
	Total																6.640	0.070		289.5	2.9
NQ103	1	2.0%	4.083	0.028	0.842	0.010	0.00029	0.00009	228.53	0.15	0.0015	0.0005	0.0030	475.20	5.66	88.7	4.305	0.183	100.0	192.9	7.8
NQ104	1	2.0%	14.657	0.039	1.798	0.011	0.00019	0.00003	17.62	0.12	0.0010	0.0002	0.0064	17.15	0.16	98.0	7.987	0.063	100.0	343.0	2.4
UM#68: J-Value[c] = 0.0262271435 ± 0.0000035669 (0.014%;1σ)																					
NQ105	1	2.0%	9.050	0.019	2.634	0.010	0.00060	0.00025	734.22	0.25	0.0032	0.0013	0.0094	487.81	1.92	89.5	3.076	0.152	100.0	140.0	6.6
NQ107	1	2.0%	38.254	0.026	5.021	0.010	0.00030	0.00007	152.89	0.13	0.0016	0.0003	0.0178	53.29	0.11	98.7	7.524	0.026	100.0	324.9	1.0
NQ108	1	2.0%	121.144	0.022	22.145	0.010	0.00076	0.00006	318.70	0.15	0.0040	0.0003	0.0786	25.19	0.02	99.0	5.416	0.005	100.0	239.6	0.2
NQ109	1	0.4%	4.556	0.028	1.083	0.004	0.00107	0.00012	284.89	0.16	0.0057	0.0006	0.0038	460.15	1.73	62.7	2.635	0.177	18.6	120.6	7.9
	2	2.0%	28.317	0.047	4.734	0.014	0.00255	0.00018	1268.01	0.37	0.0135	0.0009	0.0168	468.76	1.35	85.8	5.130	0.062	100.0	227.7	2.6
	Total																4.665	0.084		208.3	3.5
NQ110	1	2.0%	255.057	0.071	36.346	0.026	0.00090	0.00013	517.34	0.20	0.0048	0.0007	0.1290	24.91	0.02	99.4	6.978	0.008	100.0	303.2	0.3
UM#68: J-Value[c] = 0.0262369029 ± 0.0000036207 (0.014%;1σ)																					
NQ111	1	2.0%	96.965	0.025	20.318	0.017	0.00061	0.00010	264.34	0.12	0.0032	0.0005	0.0721	22.77	0.02	99.0	4.725	0.009	100.0	210.8	0.4
NQ112	1	2.0%	633.054	0.133	45.096	0.034	0.00129	0.00021	465.16	0.21	0.0068	0.0011	0.1601	18.05	0.02	99.7	13.99	0.01	100.0	564.1	0.5
NQ113	1	0.4%	2.238	0.026	0.112	0.013	0.00051	0.00004	1.39	0.12	0.0027	0.0002	0.0004	21.67	3.17	63.8	12.74	1.60	0.4	520.1	56.9
	2	2.0%	141.735	0.043	26.466	0.021	0.00069	0.00011	794.25	0.24	0.0036	0.0006	0.0940	52.52	0.05	99.2	5.314	0.008	100.0	235.5	0.3
	Total																5.346	0.015		236.8	0.6
NQ114	1	2.0%	75.773	0.023	13.956	0.009	0.00015	0.00010	214.29	0.19	0.0008	0.0006	0.0495	26.87	0.03	99.7	5.412	0.012	100.0	239.5	0.5
NQ115	1	2.0%	39.640	0.035	8.895	0.013	0.00062	0.00016	155.82	0.18	0.0033	0.0008	0.0316	30.65	0.06	97.5	4.347	0.029	100.0	194.8	1.2
UM#68: J-Value[c] = 0.0262471978 ± 0.0000036746 (0.014%;1σ)																					
NQ117	1	2.0%	18.158	0.034	5.685	0.016	0.00034	0.00014	125.90	0.20	0.0018	0.0008	0.0202	38.75	0.12	97.0	3.098	0.041	100.0	141.0	1.8
NQ118	1	2.0%	39.510	0.031	9.273	0.014	0.00060	0.00011	88.07	0.15	0.0032	0.0006	0.0329	16.62	0.04	97.6	4.159	0.021	100.0	186.9	0.9
NQ119	1	0.3%	3.892	0.012	0.774	0.012	0.00049	0.00005	16.77	0.18	0.0026	0.0003	0.0027	37.92	0.70	79.9	4.018	0.121	6.1	180.9	5.2
	2	2.0%	32.838	0.019	11.998	0.016	0.00029	0.00013	272.92	0.18	0.0016	0.0007	0.0426	39.81	0.06	98.6	2.698	0.017	100.0	123.4	0.8
	Total																2.778	0.023		127.0	1.0
NQ120	1	0.3%	1.189	0.036	0.014	0.011	0.00062	0.00005	0.14	0.08	0.0033	0.0003	0.0000	18.06	17.28	16.8	14.32	12.63	10.6	575.5	434.8
	2	2.0%	0.553	0.024	0.118	0.006	0.00013	0.00009	10.75	0.11	0.0007	0.0005	0.0004	159.53	8.80	62.7	2.941	1.189	100.0	134.2	52.3
	Total																4.145	2.401		186.3	102.4
NQ121	1	0.3%	33.056	0.046	0.127	0.005	0.00051	0.00008	1.97	0.09	0.0027	0.0004	0.0005	27.12	1.68	97.6	253.50	10.57	0.4	3671.6	65.4
	2	2.0%	183.754	0.053	31.698	0.021	0.00056	0.00021	529.32	0.27	0.0030	0.0011	0.1125	29.22	0.02	99.5	5.769	0.011	100.0	254.4	0.5
	Total																6.759	0.053		294.6	2.1
NQ122	1	0.3%	14.480	0.028	2.432	0.011	0.00031	0.00008	14.50	0.13	0.0016	0.0004	0.0086	10.43	0.10	96.6	5.755	0.056	18.3	253.8	2.3
	2	2.0%	30.718	0.032	10.821	0.013	0.00019	0.00014	134.02	0.16	0.0010	0.0008	0.0384	21.67	0.04	99.0	2.811	0.021	100.0	128.4	0.9
	Total																3.351	0.028		152.1	1.2

UM#68: J-Value[c] = 0.026247726 ± 0.0000036747 (0.014%;1σ)

NQ123	1	0.4%	3.226	0.042	0.041	0.013	0.00112	0.00007	1.85	0.12	0.0060	0.0004	0.0001	78.66	25.03	44.8	35.11	11.28	0.9	1178.3	278.0
	2	2.0%	29.964	0.035	4.622	0.006	0.00003	0.00019	1305.89	0.31	0.0002	0.0010	0.0164	494.40	0.63	99.8	6.471	0.067	100.0	283.0	2.7
	Total																6.724	0.166		293.2	6.7
NQ124	1	0.4%	160.796	0.074	0.918	0.013	0.00073	0.00010	33.67	0.09	0.0039	0.0005	0.0033	64.20	0.92	99.3	173.97	2.44	17.6	3097.1	20.8
	2	2.0%	73.977	0.050	4.310	0.014	0.00019	0.00014	335.16	0.13	0.0010	0.0007	0.0153	136.10	0.44	99.6	17.10	0.08	100.0	668.7	2.5
	Total																44.63	0.49		1399.0	10.7
NQ125	1	0.4%	7.522	0.024	1.792	0.012	0.00056	0.00009	73.75	0.14	0.0030	0.0005	0.0064	72.03	0.49	88.2	3.702	0.086	16.1	167.3	3.7
	2	2.0%	25.061	0.023	9.361	0.008	0.00013	0.00022	392.40	0.12	0.0007	0.0012	0.0332	73.35	0.07	99.2	2.655	0.037	100.0	121.5	1.7
	Total																2.823	0.045		129.0	2.0
NQ126	1	0.4%	11.966	0.042	1.825	0.007	0.00074	0.00004	27.09	0.19	0.0039	0.0002	0.0065	25.98	0.21	90.2	5.915	0.046	18.6	260.4	1.9
	2	2.0%	44.695	0.037	7.998	0.006	0.00023	0.00006	121.32	0.18	0.0012	0.0003	0.0284	26.55	0.04	99.2	5.543	0.013	100.0	245.1	0.5
	Total																5.612	0.019		247.9	0.8
NQ127	1	0.4%	14.515	0.027	1.167	0.011	0.00108	0.00009	37.20	0.21	0.0057	0.0005	0.0041	55.77	0.61	88.2	10.97	0.16	5.4	456.5	5.8
	2	2.0%	119.163	0.037	20.650	0.015	0.00051	0.00008	655.84	0.30	0.0027	0.0004	0.0733	55.58	0.05	99.3	5.731	0.008	100.0	252.8	0.3
	Total																6.012	0.016		264.3	0.639
NQ129	1	0.4%	6.432	0.015	1.271	0.011	0.00050	0.00003	31.85	0.17	0.0027	0.0002	0.0045	43.85	0.44	87.7	4.435	0.054	32.1	198.7	2.3
	2	2.0%	11.070	0.032	2.693	0.012	0.00014	0.00006	71.15	0.16	0.0008	0.0003	0.0096	46.23	0.24	97.9	4.025	0.044	100.0	181.2	1.9
	Total																4.157	0.047		186.8	2.0

UM#68: J-Value[c] = 0.026248254 ± 0.0000036675 (0.014%;1σ)

NQ130	1	0.4%	3.372	0.020	0.121	0.013	0.00021	0.00006	5.36	0.08	0.0011	0.0003	0.0004	77.21	8.44	90.3	25.09	2.83	11.4	912.7	80.7
	2	2.0%	6.279	0.021	0.942	0.013	0.00006	0.00010	59.67	0.12	0.0003	0.0005	0.0033	110.85	1.59	98.5	6.569	0.190	100.0	287.0	7.7
	Total																8.684	0.491		370.4	18.9
NQ131	1	0.4%	6.255	0.040	0.242	0.016	0.00032	0.00006	5.22	0.14	0.0017	0.0003	0.0009	37.77	2.75	91.9	23.80	1.66	2.4	875.5	48.4
	2	2.0%	83.685	0.053	9.752	0.017	0.00020	0.00006	256.01	0.16	0.0011	0.0003	0.0346	45.94	0.09	99.6	8.548	0.019	100.0	365.2	0.7
	Total																8.917	0.059		379.4	2.3
NQ132	1	0.4%	1.890	0.033	0.240	0.020	0.00043	0.00008	9.70	0.18	0.0023	0.0004	0.0009	70.67	5.92	64.1	5.044	0.695	13.4	224.3	29.0
	2	2.0%	8.796	0.038	1.554	0.018	0.00023	0.00008	73.50	0.17	0.0012	0.0004	0.0055	82.80	0.97	95.9	5.429	0.103	100.0	240.3	4.3
	Total																5.377	0.182		238.2	7.6
NQ133	1	0.4%	0.938	0.010	0.156	0.010	0.00018	0.00012	78.49	0.09	0.0009	0.0006	0.0006	882.90	58.37	70.4	4.244	1.268		190.5	54.0
NQ134	1	0.4%	3.331	0.039	0.256	0.014	0.00021	0.00005	12.21	0.10	0.0011	0.0003	0.0009	83.60	4.70	89.9	11.71	0.74	13.2	483.6	26.7
	2	2.0%	4.736	0.033	1.681	0.014	0.00006	0.00010	80.57	0.13	0.0003	0.0005	0.0060	83.88	0.71	97.9	2.757	0.096	100.0	126.0	4.2
	Total																3.939	0.181		177.5	7.7
NQ135	1	0.4%	9.831	0.025	1.920	0.008	0.00041	0.00007	17.49	0.11	0.0022	0.0004	0.0068	15.95	0.12	93.4	4.783	0.061	20.3	213.4	2.6
	2	2.0%	31.476	0.031	7.541	0.007	0.00020	0.00007	74.19	0.14	0.0011	0.0004	0.0268	17.22	0.04	99.0	4.132	0.017	100.0	185.7	0.7
	Total																4.264	0.026		191.4	1.1

[a] Data are corrected for mass spectrometer backgrounds, discrimination, radioactive decay and interference corrections. Errors are one sigma uncertainties and include uncertainties in the J-value (propagating this error only affects the third

[b] Interference corrections: $(^{36}Ar/^{37}Ar)_{Ca}$ = (2.5782 ± 0.0018) x 10^{-4}; $(^{39}Ar/^{37}Ar)_{Ca}$ = (6.5620 ± 0.0164) x 10^{-4}; $(^{40}Ar/^{39}Ar)_{K}$ = (1.00 ± 0.05) x 10^{-5}; $(^{38}Ar/^{39}Ar)_{K}$ = (1.2246 ± 0.0028) x 10^{-2}

[c] J-values calculated based on an age of 28.0200 ± 0.1597 Ma (1σ) for FC sanidine (Renne et al., 1998)

Typical blank corrections	Blank no.	^{40}Ar (fA)	±1σ	^{39}Ar (fA)	±1σ	^{38}Ar (fA)	±1σ	^{37}Ar (fA)	±1σ	^{36}Ar (fA)	±1σ
	EXB#3	0.449	0.005	-0.004	0.008	-0.062	0.036	-0.008	0.025	0.0122	0.0003
	EXB#5	0.494	0.015	-0.035	0.009	-0.069	0.031	-0.019	0.009	0.0123	0.0002
	EXB#10	0.444	0.030	-0.043	0.010	-0.019	0.018	-0.035	0.021	0.0118	0.0002
	EXB#11	0.422	0.011	-0.045	0.004	0.001	0.027	-0.016	0.008	0.0115	0.0004
	EXB#13	0.491	0.017	-0.027	0.006	-0.019	0.010	-0.011	0.017	0.0117	0.0001
	EXB#17	0.519	0.015	-0.040	0.012	-0.043	0.033	-0.003	0.021	0.0124	0.0003
	EXB#20	0.440	0.017	-0.025	0.006	-0.029	0.022	-0.011	0.021	0.0114	0.0002
	EXB#24	0.516	0.019	-0.047	0.006	-0.038	0.013	-0.012	0.015	0.0126	0.0002
	EXB#26	0.533	0.011	-0.041	0.004	-0.037	0.013	-0.006	0.007	0.0124	0.0003
	EXB#28	0.557	0.027	-0.041	0.004	-0.066	0.021	-0.022	0.019	0.0124	0.0001